JOURNAL OF GEOPHYSICAL RESEARCH, VOL. 106, NO. B1, PAGES 645–664, JANUARY 10, 2001

Depth variation of seismic anisotropy and petrology in central European lithosphere: A tectonothermal synthesis from spinel lherzolite

N. I. Christensen, L. G. Medaris Jr., and H. F. Wang

Department of Geology and Geophysics, University of Wisconsin-Madison, Madison, Wisconsin

E. Jelínek

Institute of Geochemistry, Mineralogy and Mineral Resources, Charles University, Prague, Czech Republic

Abstract. Spinel lherzolite xenoliths from the Neogene Kozákov volcano in central Europe, yielding temperatures from 680°C to 1065°C and estimated to originate from depths of 32 to 70 km, provide an exceptionally continuous record of the depth variation in seismic and petrological properties of subcontinental lithospheric mantle. Extraction depths of the xenoliths and thermal history and rheological properties of the mantle have been evaluated from a tectonothermal model for basaltic underplating associated with Neogene rifting. The chemical depletion of sub-Kozákov mantle decreases with depth, the Mg number in olivine decreasing from ~ 91.4 to 90.5 and the Cr number in spinel, decreasing from ~ 38.9 to 14.7. Texturally, the sampled mantle consists of an equigranular upper layer (32-43 km), an intermediate protogranular layer (43-67 km), and a lower equigranular layer (below 67 km). Olivine petrofabrics show strong axis concentrations, which change with depth from orthorhombic symmetry in the equigranular upper layer to axial symmetry in the lowermost layer. Calculated compressional and shear wave anisotropies, which average 8% and 6%, respectively, show significant depth trends that correlate with variations in depth of olivine fabric strengths and symmetries. Comparisons of the xenolith anisotropies with field observations of *Pn* anisotropy and *SKS* shear wave splitting in the region suggest that foliation is horizontal in the upper layer of the lithospheric mantle and vertical in the middle and lower layers. The depth variation in mantle properties and complexity in central Europe is the result of Devonian to Early Carboniferous convergence, continental accretion, and crustal thickening, followed by Late Carboniferous to Permian extension and gravitational collapse and final modification by Neogene rifting, thinning, and magmatic heating.

1. Introduction

The study of mantle seismic anisotropy beneath the continents provides earth scientists with a powerful tool for measuring and quantifying deformation in the mantle. Shear wave splitting from teleseismic phases, such as *SKS*, has become a standard method for examining upper mantle anisotropy [e.g., *Silver and Chan*, 1991; *Vinnik et al.*, 1992; *Silver*, 1996], and observations of azimuthal variations of *Pn* arrival times [e.g., *Smith and Ekström*, 1999] provide additional important constraints. Mantle anisotropy originates from the preferred alignments of minerals, predominantly olivine [e.g., *Christensen*, 1966; *Nicolas and Christensen*, 1987], and patterns of upper mantle anisotropy have been used to infer mantle strain and have been related to ancient and recent deformation of continents [e.g., *Silver and Chan*, 1991; *Savage and Silver*, 1993; *Ozalaybey and Savage*, 1994; *Savage*, 1999], to absolute plate motion [*Vinnik et al.*, 1992], and to regional convection cells [*e.g., Makeyeva et al.*, 1992; *Sandvol et al.*, 1992].

To interpret mantle anisotropy quantitatively, information is required on the fabrics of mantle peridotite and the relations between fabrics and seismic anisotropy. Peridotite xenoliths provide an important source of such data, and several investigations have established the general relations between olivine fabrics in xenoliths and calculated seismic properties [*Mainprice and Silver*, 1993; *Ji et al.*, 1994; *Kern et al.*, 1996; *Ben Ismail and Mainprice*, 1998]. However, these investigations are based on either a limited number of xenoliths from a single volcanic center or xenoliths from widely separated localities, and the depth variation in anisotropy remains to be evaluated. Twenty spinel lherzolite xenoliths from the Pliocene Kozákov volcano in central Europe, ranging in temperature from 680°C to 1065°C and estimated to originate from depths of 32 to 70 km, provide a unique opportunity to examine the depth variation in seismic and petrological properties of subcontinental lithosphere. Measurements of olivine fabrics and mineral compositions in the Kozákov xenoliths reveal a pronounced depth variation in anisotropy and mineral chemistry, which is most likely due to modification of late Variscan features by processes associated with Tertiary rifting.

Paper number 2000JB900333.
0148-0227/01/2000JB900333$09.00

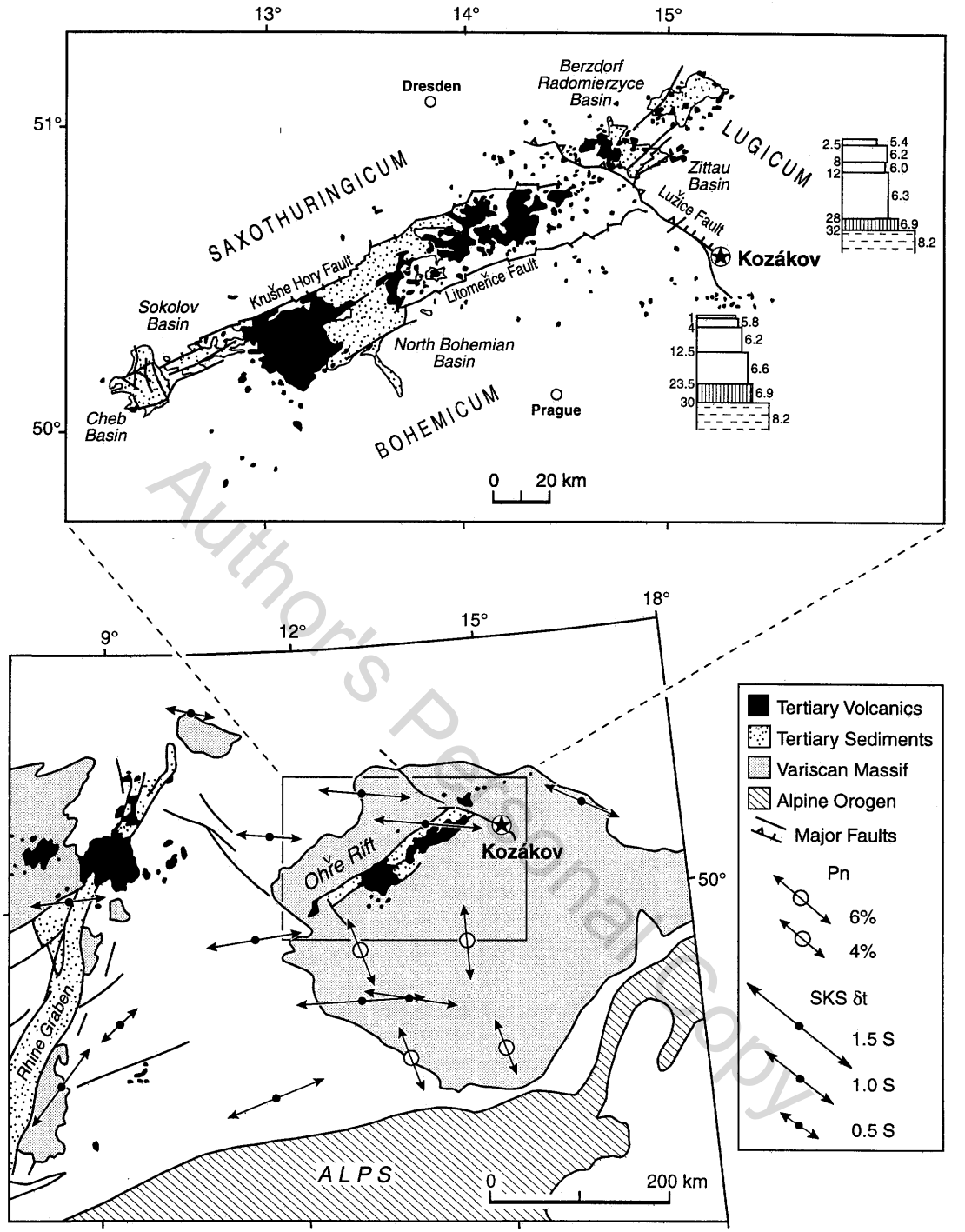

Figure 1. Simplified map of part of the European Cenozoic rift system, including the locality of Kozákov volcano and orientation and magnitude of *Pn* anisotropies and *SKS* splitting (modified from *Echtler et al.* [1994] and *Smith and Ekström* [1999]). Enlargement shows simplified geological map of the Ohře rift and representative seismic velocity-depth profiles for the Lugian and Bohemian terranes (modified from *Kasinski* [1991], and *Čermák* [1989]).

2. Geological Setting

Kozákov volcano is one of the many eruptive centers associated with the European Cenozoic rift system, which extends from the North Sea to the Mediterranean over a distance of 1100 km (Figure 1); [*Ziegler*, 1992]. The rift system evolved in the Alpine foreland during late Eocene to Recent times, and the distribution of individual grabens is controlled by tensional reactivation of basement fracture systems, which originated during the late stages of the Middle to Late Paleozoic Variscan orogeny. Changing conditions in the plate tectonic regime at the boundary of the African and European plates had a far-reaching influence on intraplate tectonics in the Alpine foreland, and the most extensive rifting took place in late Eocene time (~38 Ma), concomitant with SSW-NNE directed regional compressive stress associated

with the phase of maximum folding and overthrusting in the Alps.

The Ohře (Eger) rift, which measures ~300 km by ~30 km, is located in the northwestern part of the Bohemian Massif at the junction of three major crustal blocks, the Bohemicum, Saxothuringicum, and Lugicum (Figure 1). The southern boundary of the rift is the Litoměřice fault (Figure 1), which is of fundamental regional importance, separating the Bohemicum, composed of an anchimetamorphic Proterozoic basement and Lower Cambrian to Middle Devonian sedimentary cover, from the Saxothuringicum, consisting in the vicinity of the rift of a polymetamorphic complex, locally containing eclogite and garnet peridotite and intruded by late Variscan granitoids. The northern boundary of the rift, the Krušné Hory fault (Figure 1), lies entirely within the Saxothuringian block and has ≥1500 m of Cenozoic relief, imparting a half graben configuration to the rift, with subsidence being greater on the northwest compared to the southeast. Although the Litoměřice and Krušné Hory faults terminate at the Lužice (Lusatian) fault (Figure 1), Tertiary sedimentary and volcanic rocks extend beyond the Lužice fault to the northeast into Poland. The Lužice fault is another regionally significant Variscan structure, along which the Bohemicum and Saxothuringicum are juxtaposed against the Lugicum, a complex mosaic of predominant low- to high-grade metamorphic rocks, which locally include eclogite and garnet peridotite, subordinate Cambrian to Carboniferous sedimentary rocks, and extensive Variscan granitoids. The Lužice fault was reactivated in Cretaceous time, when the Lugian block was uplifted relative to the Saxothuringian and Moldanubian blocks, thereby exerting a significant influence on the distribution of Cretaceous sedimentation.

The Ohře rift began to subside during the late Eocene and remained active until sub-Recent time [*Kopecký*, 1986]. Several hundred meters of fluvial, alluvial, and lacustrine sediments, including important lignite deposits, accumulated in five basins, two of which are northeast of the Lužice fault (Figure 1) [*Kasinski*, 1991; *Malkovsky*, 1987]. Deposition began in the southwestern three basins in late Eocene to early Oligocene time, continued in all basins during the late Oligocene to early Miocene, and concluded in the northeastern two basins in the middle-late Miocene to Pliocene.

Four episodes of alkaline magmatism are recognized in the northern part of the Bohemian Massif, one prior to development of the Ohře rift and three related to rifting [*Ulrych et al.*, 1999]. The prerift volcanic rocks were erupted from late Cretaceous to middle Eocene time (79-49 Ma), and the synrift volcanic rocks were erupted during the late Eocene to early Miocene (43-16 Ma), middle Miocene to late Miocene (13-9 Ma), and Plio-Pleistocene (6-0.26 Ma). Among these four magmatic episodes, the late Eocene to early Miocene eruptions, which are concentrated along the rift axis (Figure 1), are the most important volumetrically, accounting for the bulk of the rift-related igneous rocks. The alkaline igneous rocks span a wide range in composition from trachyte to basalt, including an abundance of undersaturated types, such as phonolite, feldspathoidal syenite, tephrite, basanite, essexite, nephelinite, melilitite, and polzenite.

Kozákov volcano, from which the xenoliths of this investigation were collected, is situated about 30 km southeast of the Ohře rift proper, on a branch of the Lužice fault system in the Lugian block (Figure 1), and presumably taps sub-Lugian mantle. Although many alkali basalts of the Ohře rift contain mantle xenoliths, Kozákov is the most important because of the abundance and relatively large size of xenoliths there. The xenolith host is a nepheline basanite flow ~9 km long with a mean thickness of 20 m [*Fediuk*, 1994], which erupted at 4-6 Ma [*Šibrava and Havlíček*, 1980], thus belonging to the youngest of the four magmatic episodes in the Bohemian Massif.

Surface heat flow values in the central part of the Bohemian Massif are 50-60 mW m^{-2}, but relatively high heat flow values of 70-80 mW m^{-2}, and locally 90 mW m^{-2}, are observed along the Ohře rift, related to Cenozoic rifting and magmatism [*Čermák* et al., 1991]. Surface heat flow in the vicinity of Kozákov volcano is ~70 mW m^{-2}. The crust reaches a thickness of 40 km in the central Bohemian Massif but diminishes to 31 km beneath the Ohře rift and 32 km beneath Kozákov [*Čermák et al.*, 1991]. Seismic velocity-depth profiles for crust in the Bohemian and Lugian blocks [*Čermák*, 1989] on either side of Kozákov are illustrated in Figure 1. Common to both profiles is a relatively high velocity layer (6.9 km s^{-1}) at the base of the crust that may represent the crystallized products of underplated basaltic magma (see section 4.3). The lithosphere also decreases in thickness from 140 to 80 km from the central Bohemian Massif to the Ohře rift [*Čermák et al.*, 1991; *Babuška and Plomerová*, 1992].

3. Kozákov Xenoliths

The nepheline basanite lava flow at Kozákov contains abundant mantle xenoliths and rare, lower crustal xenoliths of olivine gabbronorite [*Fediuk*, 1971]. Among the mantle xenoliths, spinel lherzolite is the predominant rock type, with an average modal composition of 70% olivine, 20% orthopyroxene, 8% clinopyroxene, and 2% spinel, accompanied by subordinate harzburgite, dunite, websterite, olivine clinopyroxenite, clinopyroxenite, and orthopyroxenite [*Fediuk*, 1994]. Peridotite xenoliths are spheroidal to ellipsoidal in shape, are commonly 6-10 cm in diameter (rarely up to 70 cm), and comprise 2-3% of the lava host, with xenocrystic olivine accounting for another 7-8%. The investigated spinel lherzolite xenoliths were collected from three separate quarries at Chuchelna, Slap, and Smrčí, which are located within 4 km of each other in the same nepheline basanite flow. Kozákov xenoliths were first described by *Farsky* [1876], several rock and mineral analyses were provided by *Fediuk* [1971] and *Vokurka and Povondra* [1983], and detailed thermobarometry was performed by *Medaris et al.* [1997, 1999].

3.1. Texture

Two varieties of lherzolite occur at Kozákov (following the textural classification of *Mercier and Nicolas* [1975]): coarse- to very coarse-grained protogranular lherzolite, in which spinel occurs only in symplectic intergrowth with orthopyroxene and clinopyroxene (Figure 2, sample ORKZC3), and medium-grained equigranular lherzolite, which contains discrete, intergranular spinel (Figure 2, samples 94KZSM7, 94KZC8, and 95KZS4). In both protogranular and equigranular xenoliths, small amounts of very fine-grained silicates are present locally at spinel-pyroxene boundaries due to incipient partial fusion and

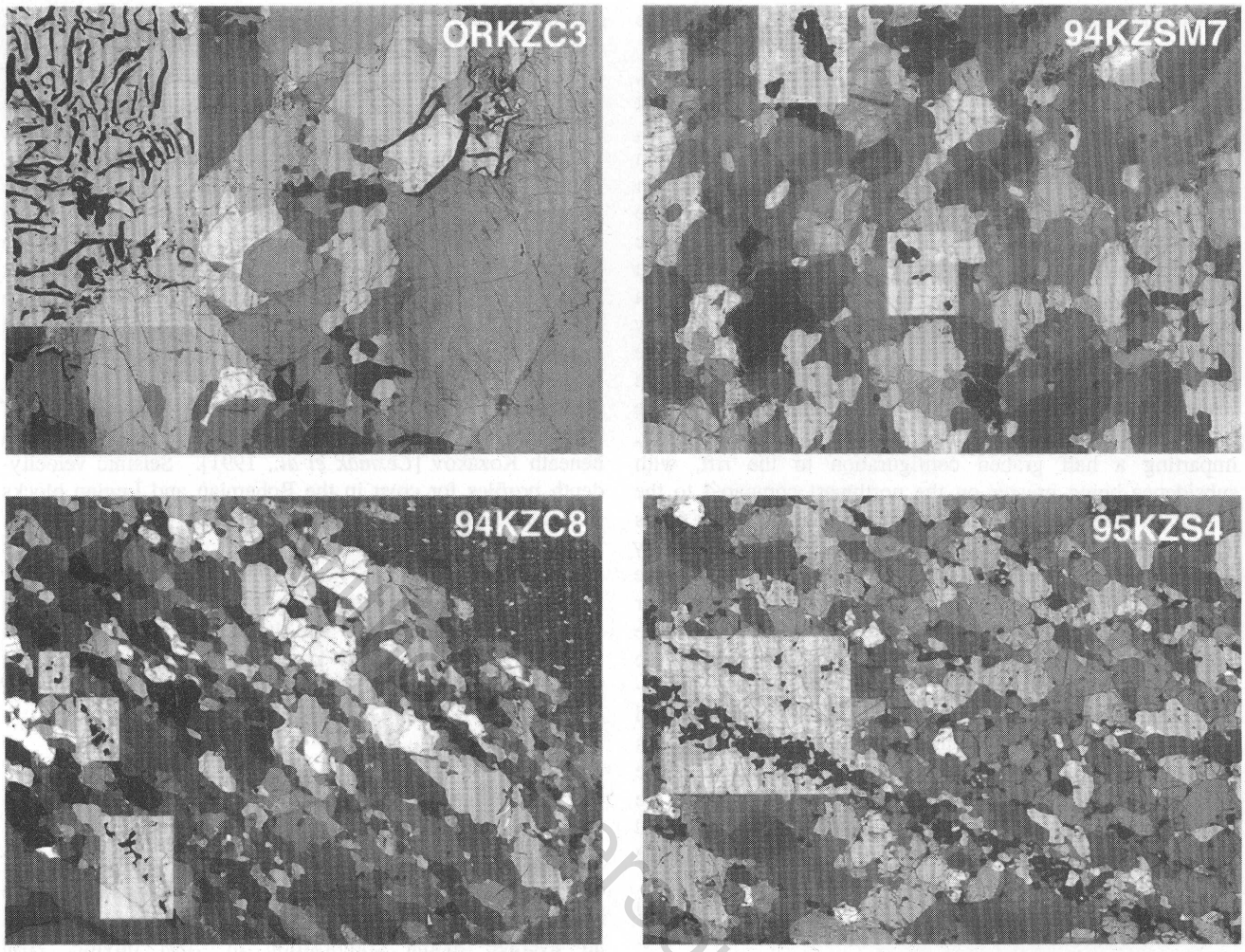

Figure 2. Photomicrographs of representative textures and fabrics in Kozákov spinel lherzolite xenoliths (partly crossed polarizers; insets with plane polarized light; width of field of view in each photomicrograph of 2 cm). ORKZC3 (930°C): typical protogranular texture with spinel-pyroxene symplectite (see inset); 94KZSM7 (1065°C) typical equigranular texture with weak foliation and discrete spinel; 94KZC8 (795°C) equigranular texture with strong foliation; and 95KZS4 (735°C) equigranular texture with foliation and prominent layering.

subsequent quenching. So far, no porphyroclastic lherzolite has been found at Kozákov.

Among 11 samples of protogranular lherzolite examined in detail, the texture is relatively consistent, being characterized by large grains, in some cases up to 2 cm in diameter, curvilinear grain boundaries, and prominent domains of spinel-pyroxene symplectite (Figure 2, ORKZC3). Based on the reconstructed bulk chemical composition of symplectite, it has been demonstrated that symplectite formed by the reaction of pre-existing garnet with matrix olivine [*Medaris et al.*, 1997], and it was suggested that such reaction was possibly promoted by heating during Neogene volcanism and accumulation of basaltic magmas at the base of the crust.

In 10 samples of equigranular lherzolite, minerals are relatively uniform in grain size (1 to 4 mm in diameter), mosaic and triple-junction grain boundaries are common, and spinel occurs as discrete, dispersed grains (Figure 2). Most samples, such as 94KZSM7, have a weak foliation and are devoid of phase layering, but sample 94KZC8 has well-developed foliation, and sample 94KZS4 has prominent spinel layering (Figure 2).

3.2. Mineralogy

Mineral compositions in 21 lherzolite xenoliths were determined by means of a Cameca SX50 electron microprobe, using an acceleration voltage of 15 kV, a beam current of 20 nA, a suite of analyzed natural minerals as standards, and the phi-rho-z data reduction program [*Armstrong*, 1988]. Complete mineral compositional data are available from L.G. Medaris.

The Kozákov lherzolite xenoliths, with one exception, are typical of group I upper mantle lherzolite [Frey and Prinz, 1978], consisting of magnesian olivine and orthopyroxene, Cr-diopside, and aluminous spinel (Table 1). The Mg numbers (= 100*Mg/(Mg+Fe)) of forsterite, orthopyroxene, and clinopyroxene are 90.2 to 91.7, 90.4 to 92.0, and 89.4 to 95.3, respectively. Orthopyroxene and clinopyroxene have a wide range in Al_2O_3 and Cr_2O_3 contents, largely reflecting a wide range in equilibration temperatures; orthopyroxene contains 1.74-5.88 wt % Al_2O_3 and 0.21-0.80 wt % Cr_2O_3, and clinopyroxene contains 2.03-6.89 wt % Al_2O_3 and 0.30-1.80 wt % Cr_2O_3. The composition of spinel varies appreciably

Table 1. Summary of Localities and Selected Features of Kozákov Spinel Lherzolite Xenoliths[a]

Sample	Quarry	Texture	Mg Number Olivine[c]	Cr Number Spinel[d]	T,[e] °C at 1.5 GPa	Max P,[f] GPa	Maximum Depth,[g] km	Model Depth,[h] km
94KZC13	Chuchelna	E	91.2	36.9	682	2.38	32.5	32.5
94KZS4	Slap	E	91.1	41.4	696	2.51	33.3	33.4
95KZS4	Slap	LE	88.2	24.1	734	1.98	36.7	36.2
94KZC4	Chuchelna	E	91.5	30.2	758	2.24	38.9	38.1
94KZC1	Chuchelna	E	91.7	43.0	775	2.62	40.4	39.4
94KZC8	Chuchelna	E	91.6	41.9	796	2.59	42.3	41.2
ORKZC7	Chuchelna	P	91.4	30.1	837	2.28	46.0	44.7
94KZSM1	Smrči	P	90.4	24.5	874	2.13	49.3	48.1
ORKZS5	Slap	P	90.8	26.2	895	2.20	51.2	50.1
95KZS3	Slap	P	90.9	25.0	921	2.19	53.6	52.7
ORKZC2	Chuchelna	P	90.7	18.6	925	2.00	53.9	53.1
ORKZC3	Chuchelna	P	91.0	21.9	931	2.10	54.5	53.7
94KZS1	Slap	P	90.8	16.8	950	1.97	56.2	55.7
ORKZS6	Slap	P	90.7	14.9	985	1.95	59.3	59.6
94KZSM6	Smrči	P	90.9	24.5	1017	2.26	62.2	63.4
94KZC16	Chuchelna	P	90.8	19.6	1033	2.13	63.7	65.4
94KZSM4	Smrči	E	91.1	25.3	1034	2.30	63.8	65.5
ORKZC6	Chuchelna	P	90.2	14.2	1045	2.00	64.8	66.9
94KZSM3	Smrči	E	90.4	18.9	1055	2.13	65.7	68.1
94KZSM5	Smrči	E	90.7	39.8	1059	2.72	66.0	68.7
94KZSM7	Smrči	E	90.5	13.6	1064	2.00	66.5	69.4

[a] Arranged in order of increasing temperature and depth.
[b] E, equigranular; LE, layered equigranular; P, protogranular.
[c] Mg number = 100 Mg/(Mg+Fe).
[d] Cr number = 100 Cr/(Cr+Al).
[e] Temperature from the two-pyroxene geothermometer of *Bertrand and Mercier* [1985].
[f] Maximum pressure calculated from spinel composition following, *O'Neill* [1981].
[g] Maximum depth determined from two-pyroxene temperature and spinel composition (see text).
[h] Depth determined from two-pyroxene temperature and model 5 Ma geotherm (see text).

among samples, with Mg ranging from 66.1 to 81.2 and Cr number (= 100*Cr/(Cr+Al)) ranging from 13.1 to 42.1. The relatively magnesian compositions of constituent minerals reflect the residual character of the xenolith bulk compositions, and the positive correlation between Mg number in forsterite and Cr number in spinel (Figure 3) indicates that variable amounts of melt were extracted from the xenolith suite, the highest degree of depletion occurring in those equigranular xenoliths with Cr number in spinel of ~40.

The single exception in the analyzed suite of lherzolite xenoliths is sample 95KZS4, which has a strong spinel layering (Figure 2, sample 95KZS4) and is likely of cumulate origin. Constituent minerals are relatively Fe-rich (Table 1), with Mg number of 88.2 for olivine, 88.4 for orthopyroxene, 90.6 for clinopyroxene, and 65.3 for spinel, and the TiO_2 content of clinopyroxene, 0.38 wt %, is distinctly higher than that in the depleted lherzolites, 0.02-0.25 wt %. In covariant plots of mineral parameters, such as Mg number of olivine versus Cr number of spinel (Figure 3), sample 95KZS4 is typically displaced from the trend of the depleted lherzolites.

4. Xenolith Temperatures, Estimated Depths, and Thermal Evolution

Equilibration temperatures of the Kozákov peridotite xenoliths have been determined by application of several appropriate geothermometers. Constraints on xenolith depths have been evaluated by combining the temperature results with the maximum pressures for stability of spinel peridotite, geothermal considerations, and geophysical data on the depth of the Moho and base of the lithosphere beneath Kozákov volcano. Xenolith depths have also been estimated by means of a magma underplating model, which has the added advantages of portraying the Cenozoic thermal evolution of the Ohře rift and providing insight into the rheological behavior of subcontinental lithosphere in a rifting environment. Both approaches yield comparable results, permitting an evaluation of the continuous depth variation of olivine petrofabrics and associated seismic anisotropy in the upper 60% of lithospheric mantle in central Europe.

4.1. Geothermometry

Temperatures have been calculated (at P = 1.5 GPa) for several domains in each of the 20 analyzed lherzolite xenoliths by two versions of the two-pyroxene geothermometer [*Bertrand and Mercier*, 1985; *Brey and Köhler*, 1990], the Al-in-orthopyroxene geothermometer [*Witt-Eickschen and Seck*, 1991], and the olivine-spinel Mg-Fe^{2+} exchange geothermometer [*Ballhaus et al.* 1991]. In general, there is excellent agreement among the different methods, reflecting the attainment and preservation of equilibrium among most elements in coexisting olivine, orthopyroxene, clinopyroxene, and spinel (see *Medaris et al.* [1999]), for a detailed comparison of results). In particular, the two-pyroxene temperatures from the *Bertrand and Mercier* [1985] and *Brey and Köhler* [1990] calibrations are consistent, with a mean difference of 36°C (2σ = 32°C) between temperatures from the two methods. Such values are

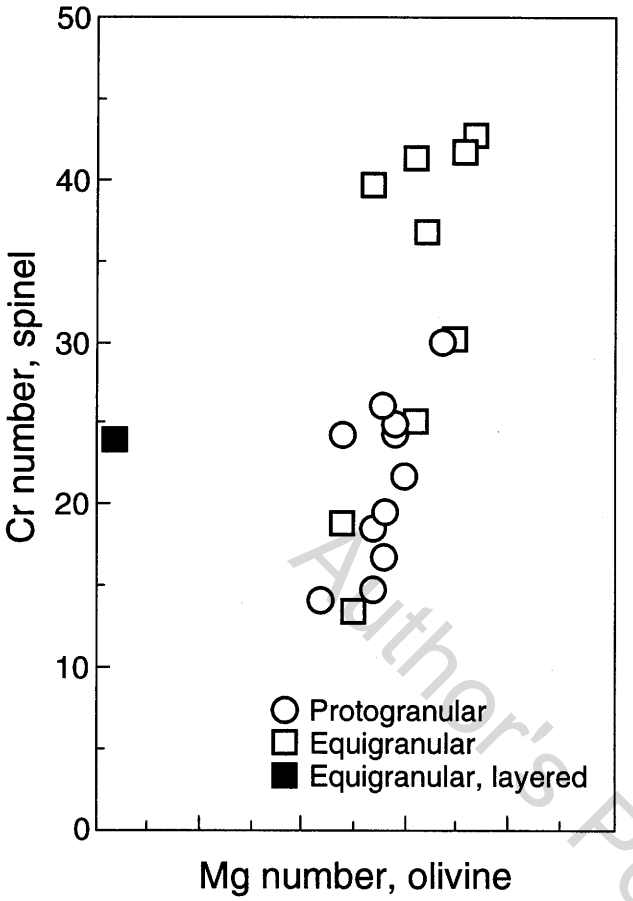

Figure 3. Correlation of Mg number in olivine, 100*Mg/(Mg+Fe), and Cr number in spinel, 100*Cr/(Cr+Al), in Kozákov lherzolite xenoliths.

comparable in magnitude to the estimated precision of the experimental calibrations of the two-pyroxene geothermometer (20°C from *Bertrand and Mercier* [1985] and 15°C from *Brey and Köhler* [1990]). The various geothermometers applied to the Kozákov xenoliths produce a wide range in temperature, from ~650 to ~1100°C, except for the Al-in-orthopyroxene geothermometer, which yields temperatures no lower than 900°C due to the relatively high blocking temperature for Al in pyroxene, compared to the other equilibria.

Two-pyroxene temperatures [*Bertrand and Mercier*, 1985] for the entire lherzolite suite range continuously from 680°C to 1065°C (Table 1), but the two different textural types fall into three groups: low-temperature equigranular (680-805°C), medium-temperature protogranular (835-1045°C), and high-temperature equigranular (1035-1065°C). The strong correlation between temperature and textural type implies that a slab of protogranular lherzolite is situated between cooler equigranular lherzolite and hotter equigranular lherzolite. Although there is an apparent overlap of protogranular and equigranular types at 1034 and 1045°C (Table 1), this is unlikely to be the case, when the precision of the two-pyroxene thermometer is taken into account.

4.2. Pressure Estimates

Pressure estimates for spinel lherzolite are currently problematic. Although a geobarometer based on the Ca content of olivine has been advocated [*Köhler and Brey*, 1990] and accurate and precise determinations of Ca in olivine can be made by electron microprobe under appropriate operating conditions, application of this geobarometer produces inconsistent and spurious results [*O'Reilly et al.*, 1996; *Medaris et al.*, 1999]. However, the maximum pressure at which spinel, rather than garnet, is the stable aluminous phase in lherzolite can be estimated from the Cr content of spinel [*O'Neill*, 1981]. Accordingly, maximum pressures for individual Kozákov lherzolite xenoliths have been calculated by *O'Neill's* [1981] method, and the results are summarized in Table 1 and plotted in Figure 4. These data can be used to place a limit on xenolith depths in the following manner: A line has been fit to the T-P_{max} coordinates of the five high-temperature xenoliths containing the most aluminous spinel with the lowest maximum pressures for a given temperature (ORKZS6, 94KZC16, ORKZC6, 94KZSM3, 94KZSM7), and the lowest temperature xenolith (94KZC13), which is assumed to occur at the top of the mantle. The resulting line, *dz/dT* in Figure 4, establishes a depth limit, below which the xenolith population could not have originated; otherwise, the spinel-garnet phase boundary constraints in the more aluminous samples would be violated. Starting from their *T*-

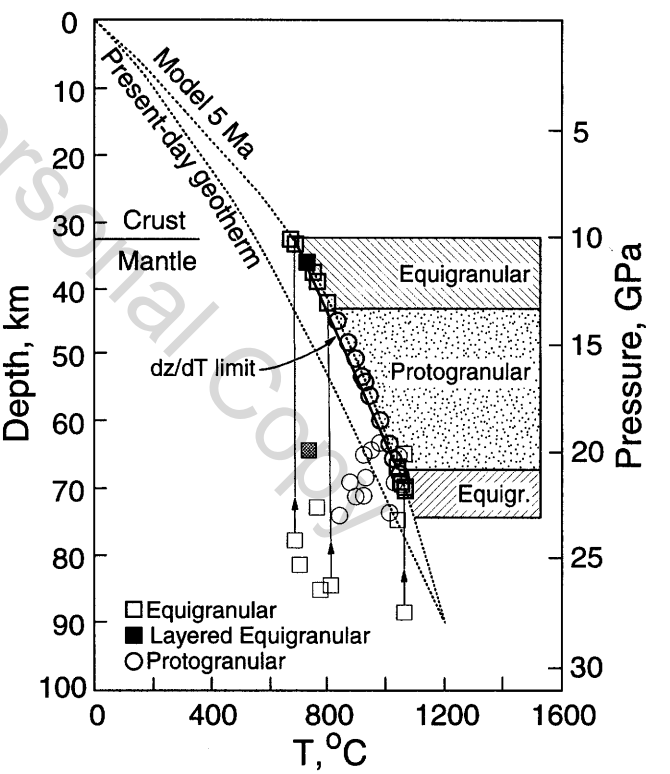

Figure 4. Maximum possible pressures and temperatures for Kozákov spinel lherzolite xenoliths (light symbols), calculated from two-pyroxene thermometry and spinel compositions [*Bertrand and Mercier*, 1985; *O'Neill*, 1981]. An estimate for the actual maximum depth limit for the xenolith suite is given by the solid line, labeled *dz/dT* limit (see text for discussion). Heavy symbols indicate estimated depths of origin, which are determined by forcing the xenoliths onto a model 5 Ma geotherm (note representative thin arrows), based on a magma underplating scenario and revealing a threefold division of the upper mantle (see text for discussion).

P_{max} loci, the xenoliths have been forced onto the limiting *dz/dT* boundary, taking into account the slight pressure dependence of the two-pyroxene geothermometer (11°C GPa^{-1}; [*Bertrand and Mercier*, 1985]), to provide an estimate of the maximum depths of origin of individual samples in the xenolith suite (Table 1).

The temperature gradient of the limiting boundary is 11.4°C km^{-1}, which when extrapolated linearly to the base of the lithosphere at 90 km (assuming a chemically depleted lithosphere with little heat-producing capacity), yields 1340°C. It is unlikely that the xenolith suite was derived from a regime in which *dT/dz* was appreciably larger than 11.4°C km^{-1}; otherwise, inordinately high temperatures would be required in the lower lithosphere. Thus the maximum depths estimated for the xenolith suite (Table 1), which range from 32.5 to 66.5 km, may also represent a reasonable approximation of the actual depths of origin.

4.3. Underplating Model

An alternative approach for estimating xenolith depths is to calculate a model geotherm for Kozákov at 5 Ma, the time of xenolith extraction, based on a magma underplating scenario. That such a process operated in the Kozákov region is suggested by the presence of lowermost crust with a relatively high seismic velocity of 6.9 km s^{-1} (Figure 1; [*Čermák*, 1989]), which may represent the crystallized products of basaltic magmas trapped at the base of the crust during culmination of Neogene magmatism, and scarce, but widespread, pyroxene granulite xenoliths thought to be samples of such underplated material [*Jakeš and Jelínek*, 1997].

The thermal evolution of lithosphere beneath Kozákov has been calculated by numerical methods for an underplating process, in which a 5-km-thick layer of basaltic magma at 1300°C accumulated at the base of the crust during the main pulse of Neogene magmatism, over a 5-Ma period between 35 and 30 Ma [*Medaris et al.*, 1999]. Initial conditions were chosen to be a 90-km-thick lithosphere and the present-day conductive geotherm (Figure 4), calculated from the following parameters: crustal thickness, 32 km; surface heat flow, 70 mW m^{-2}; mantle heat flux to the base of the lithosphere, 42 mW m^{-2}; surface radiogenic heat production, 2.0 μW m^{-3}; lithospheric mantle heat production, 0.01 μW m^{-3}; length scale of exponential decrease in crustal heat production, 7.5 km [*Čermák*, 1989; *Čermák et al.*, 1991]. Note that maximum pressures for many of the higher temperature xenoliths are less than those of the present-day geotherm (Figure 4), indicating that the thermal regime at the time of xenolith extraction (5 Ma) must have been elevated with respect to the present-day geotherm; otherwise, many of the higher-temperature xenoliths should contain garnet, rather than spinel.

The resulting geotherms at 30 Ma (the end of underplating), at 25 Ma, and at 5 Ma (the extraction time for Kozákov xenoliths) reveal the large magnitude of transient heating to be expected in the upper mantle and lower crust in response to magmatic underplating (Figure 5a). These results are similar to those obtained by *Cull et al.* [1991] for a thermal model in which 4 km of basaltic magma are injected at a temperature of 1000°C at depths between 24 and 28 km for a period of 5 Ma. Another significant implication of the thermal model is that shallow mantle was heated to higher temperatures and cooled faster than deeper mantle (Figure 5b), with predicted cooling rates of about 34°, 10°, and 3°C Ma^{-1} at depths of 35, 45, and 60 km, respectively, for the 10-Ma period following maximum heating. Such differences in cooling rates are important because of the effect on mineral equilibria, including the characteristics of pyroxene exsolution and blocking temperatures of various geothermometers.

The depths of derivation for the Kozákov xenoliths have been estimated by forcing the samples from their T-P_{max} loci onto the model geotherm calculated at 5 Ma, the time of extraction. The resulting depth estimates, ranging from 32.5 to 69.4 km (Table 1 and Figure 4), are consistent with phase petrology and the position of the crust-mantle boundary; that is, all the samples lie in the spinel field and all are situated in the mantle. In addition, the depth estimates obtained in this manner are very close to those defined by the *dz/dT* limit described in section 4.2 (compare the two sets of results in Table 1 and Figure 4). Accordingly, these model depth estimates are used in the remainder of this paper.

The underplating model has profound implications for the upper mantle with respect to its rheological properties and depth to the brittle-ductile transition. Strength envelopes for the sub-Kozákov mantle are shown in Figure 5c, calculated from the Dorn equation [*Ranalli*, 1995] using values of $10^{-14}s^{-1}$ for strain rate and 2.5×10^4 MPa^{-n} s^{-1}, 3.5, and 530 kJ mol^{-1} for the Dorn parameter, stress exponent, and creep activation energy, respectively, for dry olivine (summarized by *Evans and Kohlstedt* [1995]). At the end of magmatic underplating at 30 Ma, heating would have reduced the ductile strength of the entire upper mantle to values < 50 MPa (which is commonly taken as a threshold level delimiting the mechanically strong part of the lithosphere [*Cloetingh and Banda*, 1992]), and restoration of a brittle regime for the uppermost mantle would not have begun until about 20 Ma, i.e., 10 Ma after the cessation of underplating. With further cooling and thermal readjustment, the brittle-ductile transition would have moved to progressively deeper levels, until reaching the present-day depth of ~59 km.

5. Olivine Petrofabrics

Fifteen xenolith samples, originating from estimated depths of ~32 km to 70 km, were selected for petrofabric analysis using a five-axis universal stage. Thin sections were cut from each sample and orientations of the crystallographic axes of olivine grains were determined using the techniques of *Emmons* [1943]. Between 100 and 150 olivine grains were selected for orientation from each specimen. Results of the petrofabric studies are presented in Figure 6 as lower hemisphere plots of the concentrations of olivine crystallographic axes. For each sample, maximum concentrations of olivine *a* axes, [100], and *c* axes, [001], were rotated into an arbitrary plane of the projection, in which the *a* and *c* axes maximum concentrations are east-west and north-south, respectively.

The most consistent feature of the petrofabric analyses is the strong concentration of olivine *b* axes, [010], in each sample. Crystallographic *b* is the slowest propagation direction for seismic waves in single crystal olivine [*Verma*, 1960; *Kumazawa and Anderson*, 1969], and the concentrations of these axes impose a seismic anisotropy on

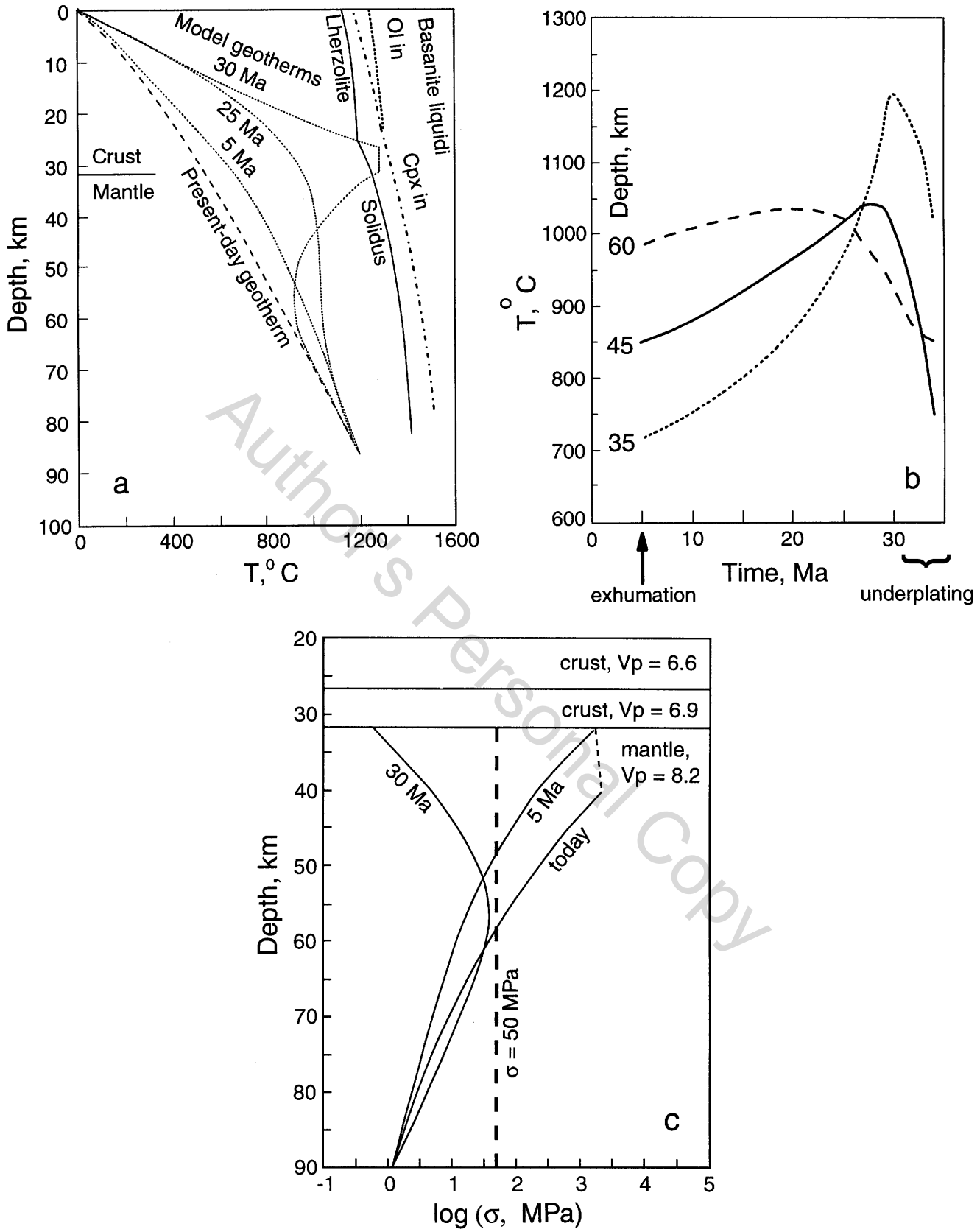

Figure 5. Summary of important results from the magmatic underplating model. (a) Geotherms at 30 Ma (end of underplating), 25 Ma, and 5 Ma (time of extraction). (b) Cooling histories for mantle at depths of 35, 45, and 60 km. (c) Depth dependent rheology of sub-Kozákov mantle at 35 Ma, 5 Ma, and present-day, based on the magmatic underplating model. A threshold level delimiting mechanically strong lithosphere is taken to be 50 MPa.

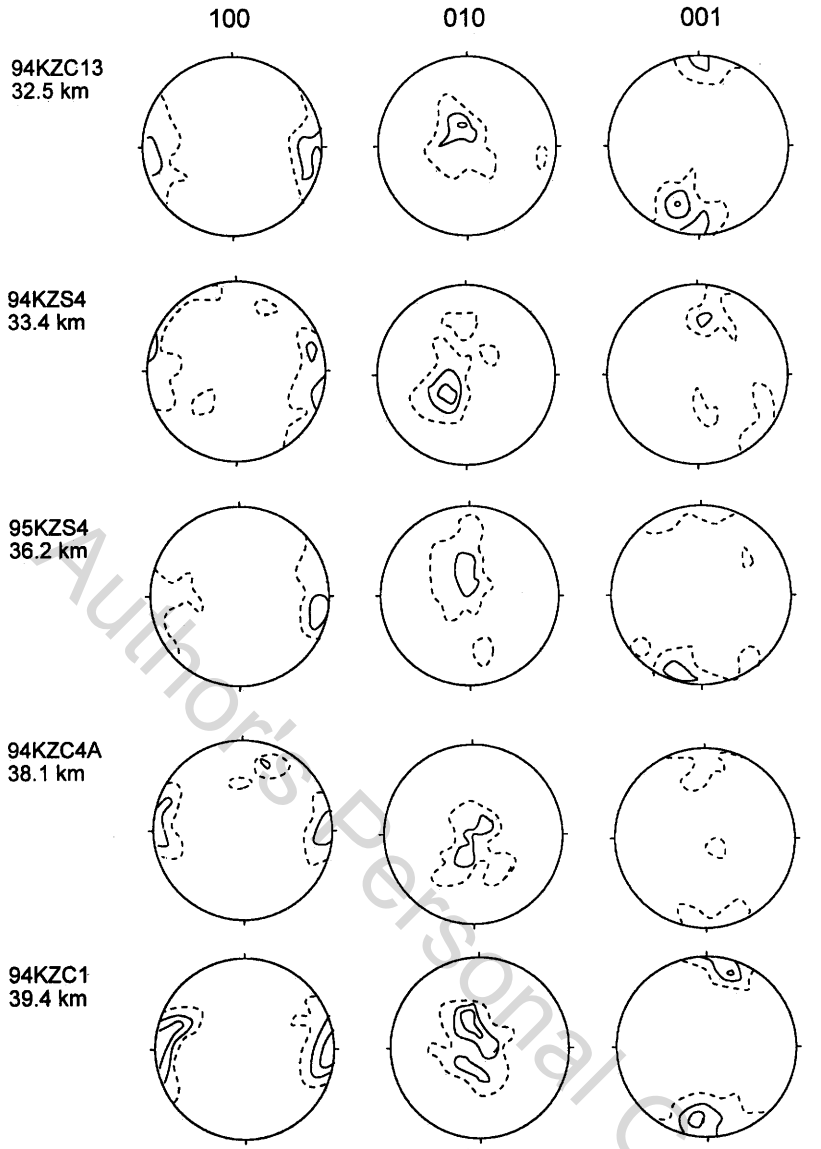

Figure 6. Equal-area, lower hemisphere projections of [100], [010], and [001] axes of olivine. Contour intervals are 2% per 1% area, and the lowest contours are shown as dashed lines. Foliations are approximately in the plane of the paper, and lineations, where present, are parallel to olivine [100] axes maxima.

the samples. Furthermore many of the samples, especially from the upper 20 km of the section, show strong concentrations of olivine *a* and *c* axes and have orthorhombic symmetries. The olivine axes concentrations are generally stronger in the upper section, which results in relatively high seismic anisotropy. The olivine *a* and *c* axes in the two lowermost samples (94KZSM5 and 94KZSM7) girdle around strong *b* axes concentrations, producing axial symmetries.

The orthorhombic symmetries observed in the uppermost samples are consistent with fabrics produced by axial deformation experiments [*Carter and Ave'Lallemant*, 1970; *Nicolas et al.*, 1973] at high temperatures in which olivine deforms by plastic flow on the slip system (010) [100]. Similar fabrics have been produced in synthetic olivine aggregates deformed in simple shear experiments [*Zhang et al.*, 2000] and reported in peridotites from ophiolites [e.g., *Christensen and Salisbury*, 1979; *Christensen*, 1984], massif peridotites [*Christensen and Crosson*, 1968], and upper mantle xenoliths from the Sierra Nevada [*Peselnick et al.*, 1977], South Africa [*Mainprice and Silver*, 1993], the Canadian Cordillera [*Ji et al.*, 1994], and Baikal, Russia [*Kern et al.*, 1996].

6. Seismic Anisotropy

The olivine orientation measurements have been used to calculate the seismic anisotropies of each sample using the elastic constants of olivine. Calculations of anisotropy from petrofabric data were first presented by *Kumazawa* [1964] for hypothetical olivine aggregates having relatively simple symmetry patterns. Early calculations of velocity anisotropy from olivine petrofabric data were found to agree well with laboratory-measured velocity anisotropies [e.g., *Klima and Babuška*, 1968; *Crosson and Lin*, 1971; *Baker and Carter*,

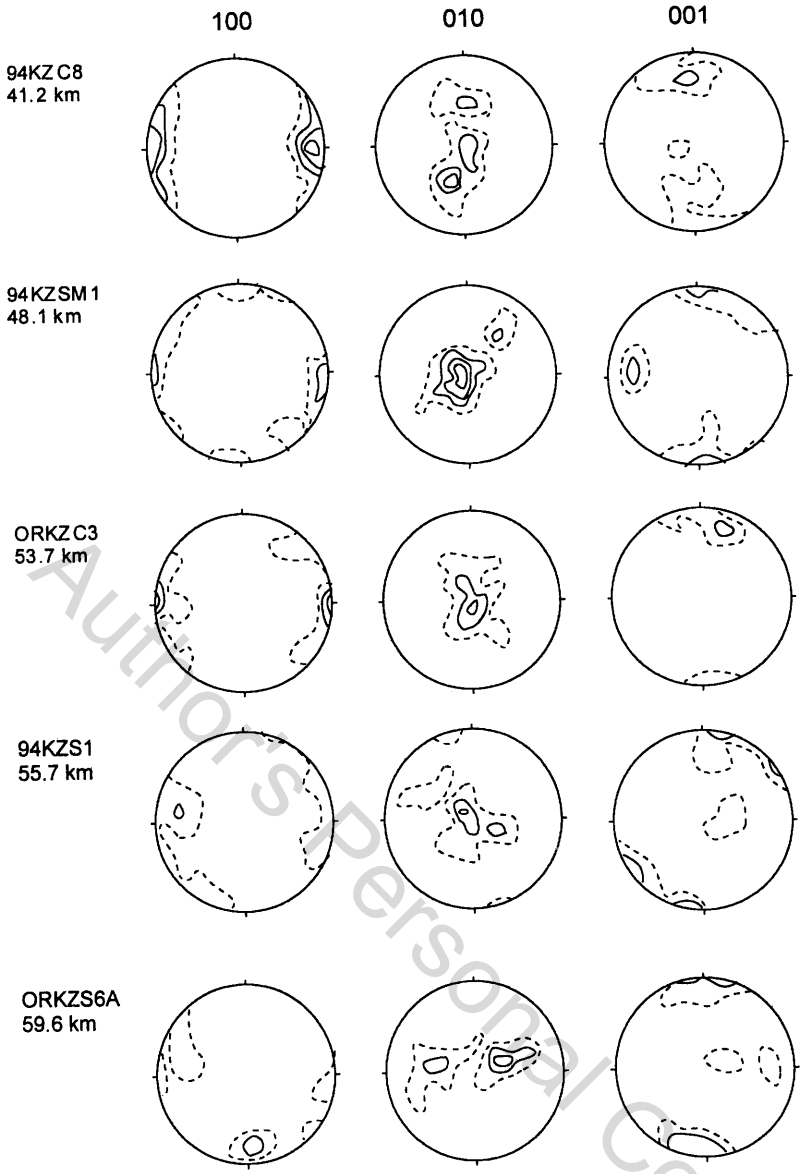

Figure 6. (continued)

1972; *Babuška*, 1972]. The general procedure used to calculate velocity anisotropy obtains mean values of elastic constants according to the Voigt or Reuss methods [e.g., *Crosson and Lin*, 1971] but with weights found from the petrofabric data. This produces a set of elastic constants from which velocities for the aggregate are then calculated from the general equations for plane waves in anisotropic media.

The velocity anisotropies presented in Figure 7 have been obtained using a slightly modified version of the technique described by *Crosson and Lin* [1971], the elastic constants of olivine and their pressure and temperature derivatives [*Kumazawa and Anderson*, 1969; *Suzuki and Anderson*, 1983], the olivine petrofabric data for each sample, and the density of olivine. The solution of the Cristoffel equation for any given wave normal gives three velocities which correspond, in general, to one quasi-compressional and two quasi-shear waves [e.g., *Musgrave*, 1970]. The two quasi-shear waves are orthogonally polarized and travel at different velocities for most propagation directions. Contour diagrams of compressional wave velocities, the difference in velocity between the two quasi-shear waves, which is a measure of shear wave splitting, the time difference between the two quasi-shear wave arrivals traveling through a 100-km-thick mantle slab, and the vibration directions of the fast quasi-shear wave are shown in Figure 7 for each sample. Orientations correspond to those of the petrofabric diagrams of Figure 6 and are presented in order of increasing estimated depth.

The seismic velocities and anisotropies of Figure 7 are for 100% olivine (dunite). Pyroxene and accessory spinel do not significantly affect the symmetry patterns in Figure 7, but they will lower velocities and anisotropies. This relation between pyroxene content and seismic anisotropies of olivine-pyroxene assemblages has been investigated in detail by *Christensen and Lundquist* [1982], using multiple field oriented samples in large peridotite massifs.

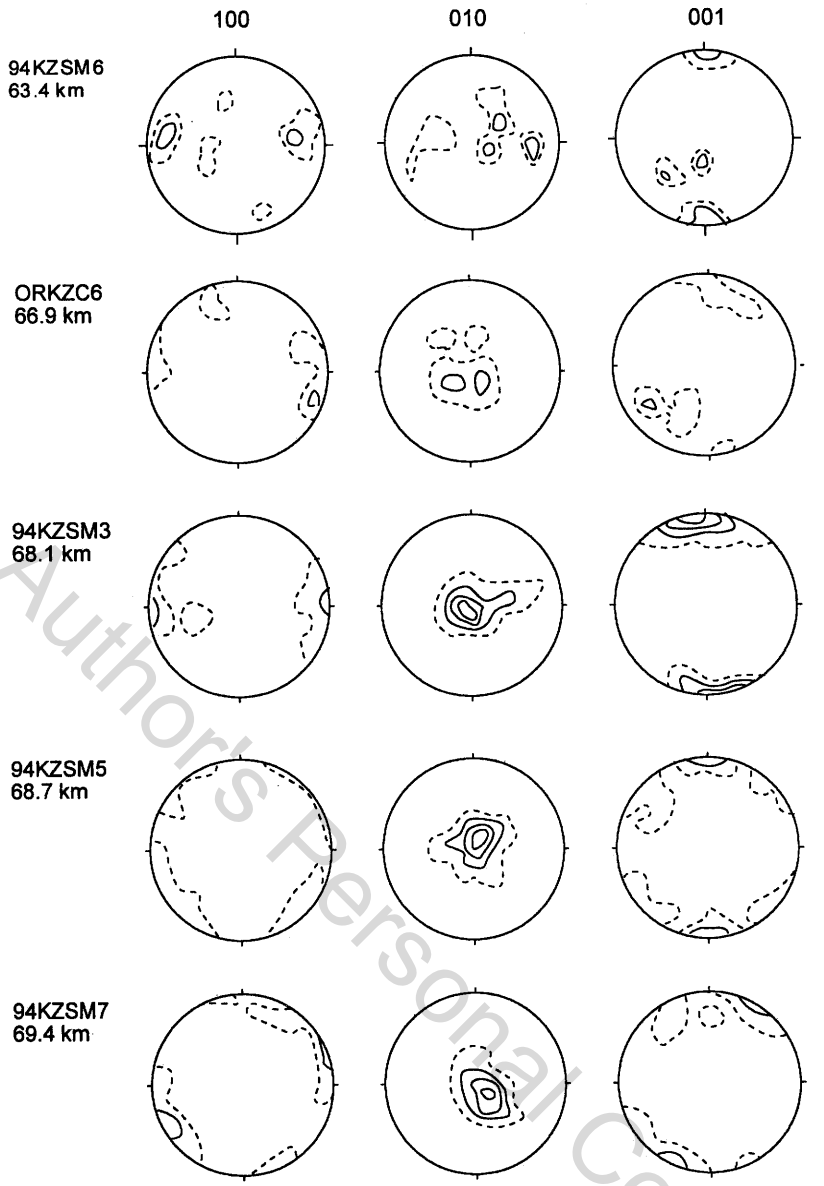

Figure 6. (continued)

7. Depth Variation of Petrological and Seismic Properties

The excavation of Kozákov lherzolite xenoliths from a continuous range of estimated depths from immediately below the Moho at 32 km to 70 km provides an exceptional opportunity to assess the depth variation of compositional and seismic properties of subcontinental lithosphere in central Europe. The lithosphere beneath Kozákov volcano is estimated to be 90 km thick, based on surface wave data [*Panza*, 1985], and the xenoliths provide direct evidence of mantle characteristics for the upper 60% of the lithospheric mantle.

A prominent feature of the sub-Kozákov lithosphere is the occurrence of a 23-km-thick layer of protogranular lherzolite sandwiched between shallower and deeper layers of equigranular lherzolite (Figures 4 and 8). Within this tripartite structure of the upper mantle, there is a continuous change in chemical composition, as reflected in the compositions of olivine and spinel (Figure 8 and Table 1). Overall, the Mg number of olivine decreases with depth, as does the Cr number of spinel (except for one high-temperature equigranular sample), indicating that shallower samples are chemically more depleted than are deeper samples. Such a chemical variation with depth has been detected elsewhere and seems to be generally characteristic of subcontinental upper mantle [*Griffin et al.*, 1998].

Total rock anisotropies are tabulated in Table 2 in order of increasing estimated depth. For each rock we computed the maximum (V_p max) and minimum (V_p min) compressional wave velocities and the compressional wave anisotropy (V_p aniso), defined as V_p max - V_p min expressed as a percentage of the average of V_p max and V_p min. Also given in Table 2 are the fast (V_s fast) and slow (V_s slow) shear wave velocities corresponding to the direction of maximum shear wave splitting and the shear wave splitting (ΔV_s). Comparisons of

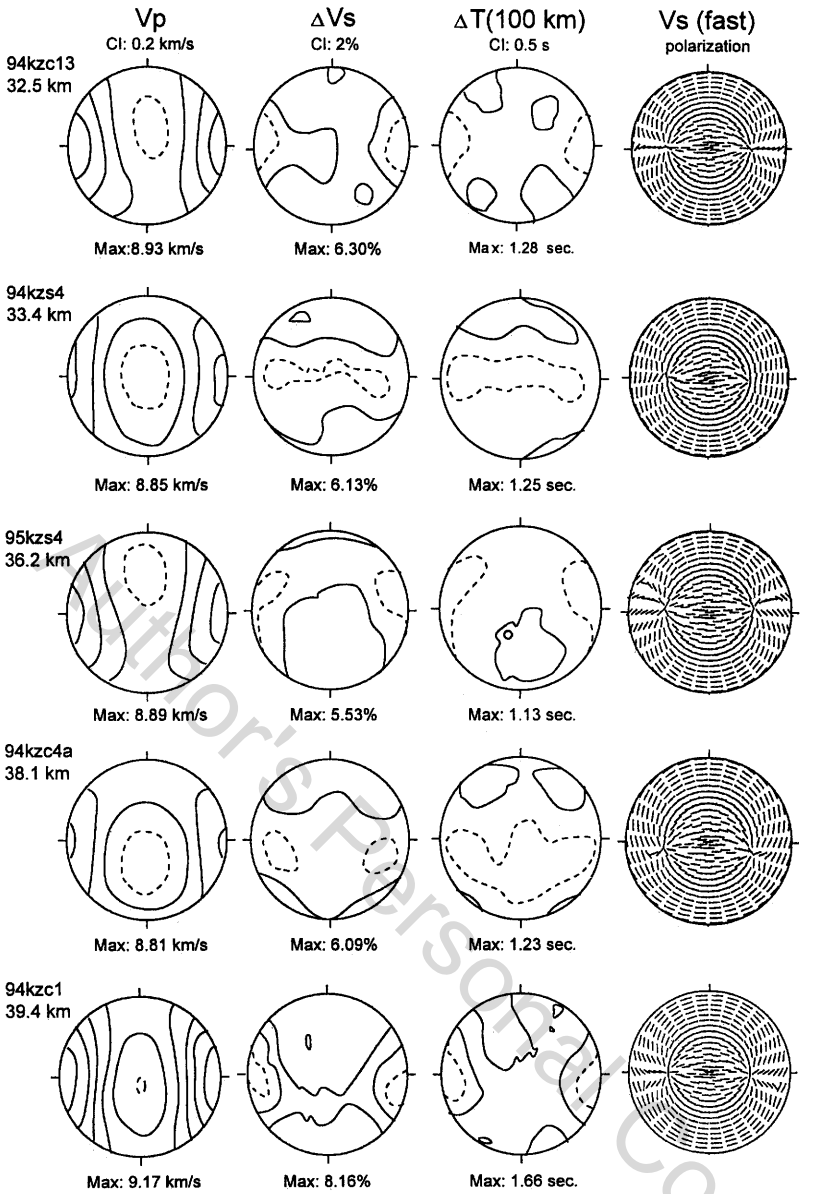

Figure 7. Compressional wave velocity (V_p) in km s^{-1}, shear wave splitting (ΔV_s) in %, arrival time differences (ΔT) in s. of split shear waves for a 100-km-thick slab and fast shear wave polarization directions.

xenolith anisotropies with field-based measurements are complicated because information does not exist on the relative orientations of samples from similar depths. Owing to possible variations in geographic crystallographic orientations of olivine and pyroxene among individual samples, anisotropies may be somewhat less than those calculated from individual samples. This has been observed in anisotropy studies of large ophiolite massifs [*Christensen*, 1984].

Both the compressional and shear wave anisotropies of Table 2 show significant depth trends (Figure 8) which correlate with depth variations in olivine fabric strengths and symmetries discussed in section 5. In the upper 10 km of mantle sampled by six xenoliths (94KZC13 through 94KZC68, Table 1) V_p anisotropy and shear wave splitting percentages are relatively high. For these samples olivine *a*, *b*, and *c* axes form strong mutually perpendicular maxima giving rise to orthorhombic symmetries. These fabrics and their associated strong anisotropies are likely related to Pn anisotropies observed in the region.

The change in fabric strength of olivine *a* axes is primarily responsible for the decrease of anisotropies with estimated depth in xenoliths from the protogranular lherzolite region (Figure 8). Also the decreases with depth in V_p and V_s anisotropies of this region correlate well with the observed decrease in Cr number of spinel with depth. The lowermost transition from protogranular to equigranular texture at ~66 km depth is also accompanied by significant changes in V_p and V_s anisotropies. The two xenoliths originating from the greatest depths (94KZSM5 and 94KZSM7) are equigranular and have olivine fabrics which produce approximate transverse isotropy (Figure 7) with slow symmetry axes corresponding to olivine *b* axes maxima concentrations. This

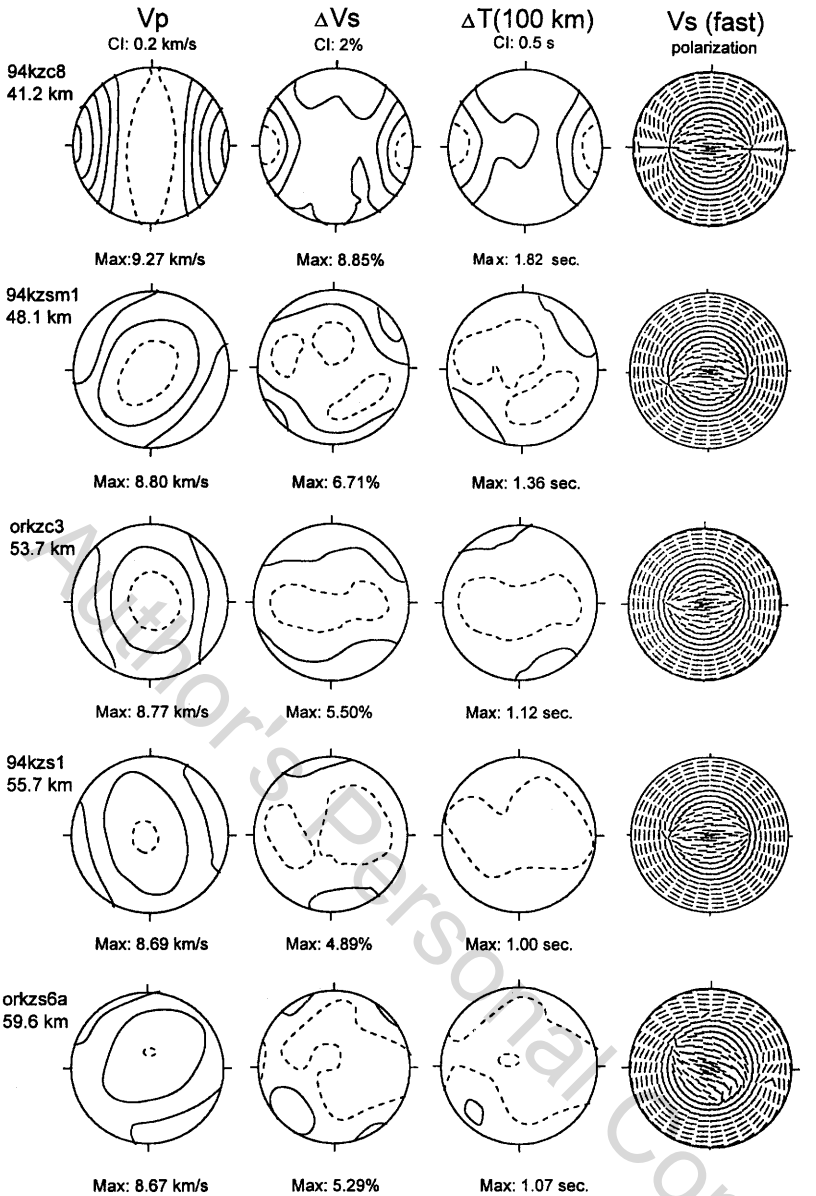

Figure 7. (continued)

symmetry originates from the strong olivine *b* axis concentrations coupled with well defined olivine *a* and *c* axes girdles.

8. Origin and Significance of Sub-Kozákov Mantle Properties

8.1. Tectonic Influence on Mantle Evolution

The crust and mantle of the Bohemian Massif were profoundly affected by Variscan tectonics, most notably Devonian to Early Carboniferous convergence (~340-360 Ma), which led to accretion of continental fragments and associated crustal thickening and high-pressure metamorphism. Convergence was followed by widespread Late Carboniferous to Permian post-thickening extension and gravitational collapse (~280-300 Ma), which resulted in restoration of a normal crustal thickness and a flat Moho, horizontal seismic layering of the lower crust, bimodal volcanism, medium-pressure high-temperature metamorphism of the lower crust, and extensive intermontane basins dominated by continental clastic deposits [*Giese*, 1995; *Franke et al.*, 1995; *Lorenz and Nicholls*, 1976; *Rey*, 1993; *Costa and Rey*, 1995]. Subsequently, lithosphere in the Bohemian Massif was further thinned and modified locally by Neogene rifting, which produced the Ohře half graben and its associated alkaline volcanic rocks and sedimentary basins.

Thus the gross mantle structure beneath Kozákov volcano, as revealed by lherzolite xenoliths, is most likely the product of Variscan tectonics. It has been demonstrated that protogranular spinel lherzolite originally consisted of garnet lherzolite [*Medaris et al.*, 1997], and we suggest that the tripartite structure of the mantle resulted from Variscan convergence and imbrication, in which protogranular metastable garnet lherzolite was sandwiched within equigranular spinel lherzolite, representing a mantle analogue

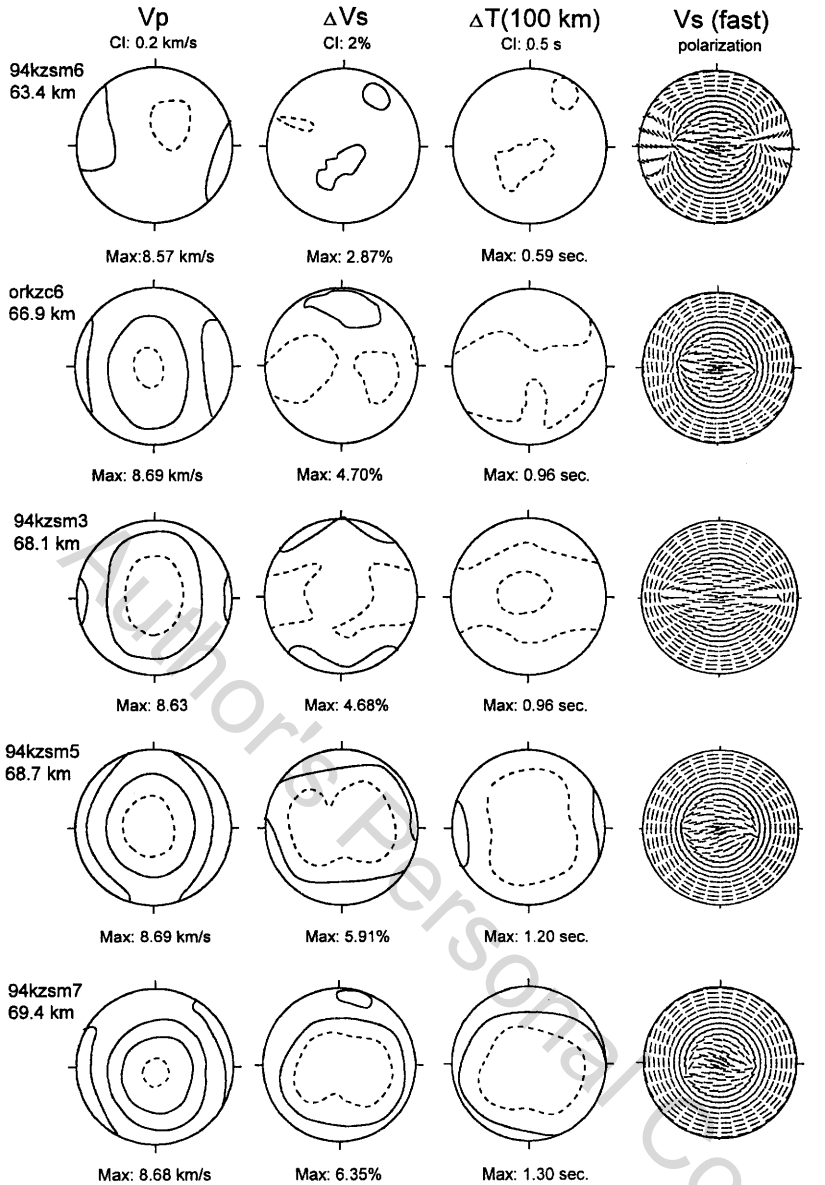

Figure 7. (continued)

of the well-documented Variscan tectonic juxtaposition of mantle-derived garnet lherzolite with continental crust [*Carswell,* 1991; *Medaris et al.*, 1990]. Subsolidus reaction of garnet with matrix olivine to produce pyroxene-spinel symplectite could have been promoted by the thermal pulse associated with either Permocarboniferous extension or Neogene underplating. However, garnet recrystallization occurred after the last significant internal deformation in protogranular lherzolite because the original grain shapes of garnet are preserved by pyroxene-spinel symplectite (Figure 2, sample ORK2C3). Consequently, it is most reasonable to call upon Neogene heating as the effective agent for promoting reaction between garnet and olivine.

Although the gross structure of the sub-Kozákov mantle can be ascribed to Variscan tectonics, Neogene underplating and heating would have had a profound influence on mantle properties, and the estimated extraction depths for the Kozákov lherzolite xenoliths are critically dependent on our underplating model. The question then arises as to whether Neogene heating did, in fact, occur. Several lines of evidence provide support for the existence of a thermal pulse in Neogene time:

1. Higher-temperature xenoliths yield comparable results from two-pyroxene, olivine-spinel, and Al-in-orthopyroxene geothermometers, but lower-temperature xenoliths show a discrepancy between two-pyroxene and olivine-spinel geothermometers, which yield temperatures down to 680°C, and the Al-in-orthopyroxene geothermometer, which yields a minimum temperature of 900°C [*Medaris et al.*, 1999]. Such discrepancy is most likely due to heating of the shallow mantle above 900°C, followed by rapid cooling of the order of 30°C Ma^{-1} (Figure 5b), during which Ca, Mg, and Fe reequilibrated among orthopyroxene, clinopyroxene, olivine, and spinel down to temperatures below 700°C, but the more slowly diffusing Al was "frozen" in the pyroxenes at about 900°C.

2. Pyroxene exsolution lamellae in deep xenoliths are uncommon, relatively thick, and sharply defined, in contrast

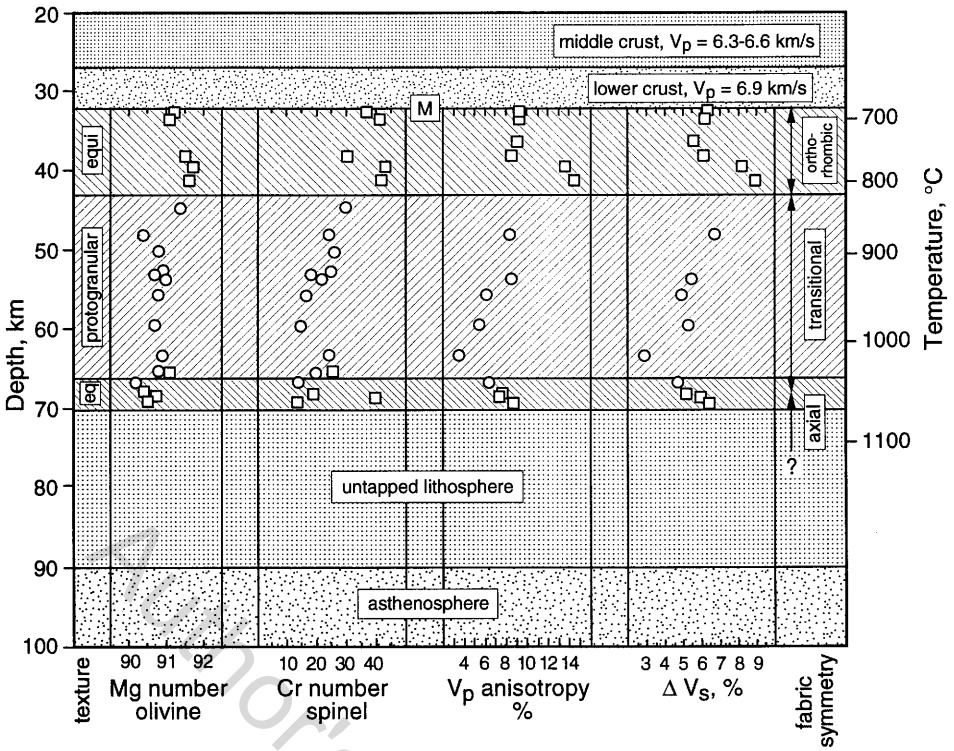

Figure 8. Variations with estimated depth and temperature of Mg number in olivine, Cr number in spinel, V_p anisotropy, ΔV_s, and fabric symmetry in Kozákov spinel lherzolite xenoliths.

to those in shallow xenoliths, which are abundant, relatively thin, and diffuse. In addition, pyroxene hosts in exsolved grains are compositionally more homogeneous in deep samples compared to shallow. Such differences are consistent with cooling rates predicted by the underplating model. Cooling in deeper samples was slow enough to allow for extensive reequilibration and reorganization of pyroxene components, but faster cooling at shallow levels resulted in arrested reequilibration.

3. Most of the rock types that occur in outcrops of Variscan basement, including high-pressure high-temperature garnet granulite, occur as xenoliths in Neogene volcanics of the Ohře rift. However, low-pressure high-temperature pyroxene granulite has been identified only in xenoliths, never in outcrop, and is thought to represent the metamorphism of lower continental crust during Neogene heating [*Jakeš and Jelínek*, 1997].

4. Olivine fabrics in equigranular lherzolite xenoliths from estimated depths of 32 to 42 km have a well-defined orthorhombic symmetry. The presence of such symmetry, which is characteristic of high-temperature plastic deformation [*Carter and Ave'Lallemant*, 1970], in the shallow equigranular xenoliths implies that they experienced high-temperature deformation prior to cooling to temperatures ranging from 680 to 795°C.

8.2. A Model for Mantle Structure Beneath Kozákov Volcano

Early studies of mantle shear wave splitting found that in mountain belts motions of the fast shear waves are commonly aligned with the strikes of the orogens [e.g., *Silver and Chan*, 1988; *Vinnik et al.*, 1992]. Time differences in arrivals of the split shear waves were initially interpreted to originate from a mantle slab of uniform anisotropy extending from the Mohorovicic discontinuity to the base of the lithosphere. As the quality and quantity of shear wave splitting observations increased, it became apparent that upper mantle anisotropy varies with depth [e.g., *Savage and Silver*, 1993; *Babuška et al.*, 1993; *Vinnik et al.*, 1994; *Bormann et al.*, 1996], can show great lateral variability [e.g., *Plomerová et al.*, 1988] and may extend well into the asthenosphere [e.g., *Plomerová et al.*, 1998; *Levin et al.*, 1999]. In the previous sections we have shown that the Kozákov xenoliths show systematic changes in magnitude and symmetry of anisotropy with temperature and estimated depth. Correlation of these observations with field-based seismic observations and tectonic models of central Europe provides constraints on understanding the present-day record of active and past mantle deformations recorded by mantle anisotropy.

Several investigations of *SKS* shear wave splitting have been reported in the vicinities of the Ohře rift and Rhine graben [*Bormann et al.*, 1996; *Silver and Chan*, 1991; *Vinnik et al.*, 1992, 1994; *Plomerová et al.*, 1988]. These studies show that the mantle beneath this region is highly anisotropic with the dominant direction of the fast shear wave motion E-W near the Ohře rift (Figure 1). To the southwest, toward the Rhine graben, the fast polarizations swing to a NE-SW orientation approximately parallel to the rift zone. Although there is some variability, delay times average ~1s. *Pn* anisotropies of 4.1 to 5.0% have been reported south of the Ohře rift [*Smith and Ekstrom*, 1999]. The direction of maximum *Pn* velocity is NW-SE at a high angle to the trend of the Ohře rift and to the shear wave splitting fast polarization directions (Figure 1). An earlier regional study

Table 2. Whole Rock Compressional Wave (V_p) and Shear Wave (V_s) Anisotropies

Sample	Depth, km	V_p Max km s^{-1}	V_p Min km s^{-1}	V_p Aniso, %	*Vs* Fast, km s^{-1}	*Vs* Slow, km s^{-1}	ΔV_s, %
94KZC13	32.5	8.93	8.14	9.26	5.07	4.76	6.31
94KZS4	33.4	8.86	8.08	9.21	5.04	4.74	6.13
95KZS4	36.2	8.89	8.12	9.05	5.03	4.76	5.52
94KZC4a	38.1	8.82	8.10	8.51	5.09	4.79	6.07
94KZC1	39.4	9.17	8.00	13.63	5.08	4.68	8.20
94KZC8	41.2	9.27	8.02	14.46	5.06	4.63	8.88
94KZSM1	48.1	8.80	8.09	8.41	5.08	4.75	6.71
ORKZC3	53.7	8.77	8.05	8.56	5.05	4.78	5.49
94KZS1	55.7	8.70	8.18	6.16	5.02	4.78	4.90
ORKZS6a	59.6	8.67	8.20	5.57	5.03	4.77	5.31
94KZSM6	63.4	8.57	8.27	3.56	4.94	4.80	2.87
ORKZC6	66.9	8.70	8.16	6.41	5.01	4.78	4.70
94KZSM3	68.1	8.73	8.10	7.49	5.02	4.77	5.11
94KZSM5	68.7	8.69	8.07	7.40	5.05	4.76	5.91
94KZSM7	69.4	8.68	7.96	8.65	5.03	4.72	6.36
Average	51.6	8.82	8.10	8.42	5.04	4.75	5.92

by *Bamford* [1977], using quarry blast observations, reported 6 to 7% anisotropy, with the maximum velocity 20°E in western Germany. The lower crust in the region of the Ohře rift is characterized by strong horizontal reflections [*Giese*, 1995], suggesting horizontal foliations at and near the Moho.

Laboratory measurements of velocities in anisotropic peridotites and calculated seismic properties have shown that vibration directions of fast shear waves parallel fast compressional wave propagation directions [e.g., *Christensen and Ramananantoandro*, 1971; *Mainprice and Silver*, 1993; *Ben Ismail and Mainprice*, 1998]. This is also illustrated by a comparison of the V_p anisotropy calculations of Figure 7 with the fast shear wave polarization directions. The differences between the fast *Pn* velocity directions shown in Figure 1 beneath the Bohemian Massif and the fast polarization directions of shear wave splitting are explained by a depth dependent anisotropy model [*Vinnik et al.*, 1994]. *Pn* velocity measurements provide anisotropy information on mantle immediately beneath the Mohorovicic discontinuity, whereas *SKS* shear wave splitting observations sample the whole mantle

We have shown that Kozákov xenoliths from the upper 10 to 15 km of the mantle have relatively high anisotropies and orthorhombic symmetries. The magnitude of *Pn* anisotropy predicted from our observations depends on the insitu orientation of the xenoliths. In Table 3 we have calculated *Pn* anisotropies for three different orientations: horizontal foliation (olivine *b* axes maxima vertical), vertical foliation with olivine *c* axes maxima vertical, and vertical foliation with olivine *a* axes maxima vertical. These anisotropies are for rocks with 100% olivine (dunite) and will be lowered by the presence of pyroxene and other accessory minerals. Using the relationships between anisotropy and pyroxene content of peridotites observed by *Christensen and Lundquist* [1982], we have calculated average *Pn* anisotropies for the upper 15 km of the mantle sampled by our xenoliths, assuming an average pyroxene content of 25%. All pyroxene has been assumed to be orthorhombic; no garnet occurs in the xenoliths. Using these adjusted values, horizontal foliation produces 5.6% *Pn* anisotropy, which is in excellent agreement with the observed *Pn* ANISOTROPY in the region (Figure 1), whereas vertical foliation with olivine *c* axes maxima vertical and olivine *a* axes maxima vertical give *Pn* anisotropies of 8.0% and 2.5%, respectively.

We attribute the observed olivine fabrics and associated anisotropy in this region of the upper mantle to originate from

Table 3. Compressional Wave Velocity (V_p) Anisotropies for *Pn* Observations as a Function of Foliation Orientation

		Horizontal Foliation (Olivine *b* Maxima Vertical)			Vertical Foliation (Olivine *c* Maxima Vertical)			Vertical Foliation (Olivine *a* Maxima Vertical)		
Sample	Depth, km	V_p Max, km s^{-1}	V_p Min, km s^{-1}	Aniso, %	V_p Max, km/s	V_p Min, km s^{-1}	Aniso, %	V_p Max, km s^{-1}	V_p Min, km s^{-1}	Aniso, %
94KZC13	32.5	8.93	8.30	7.3	8.93	8.14	9.3	8.34	8.14	2.4
94KZS4	33.4	8.85	8.41	5.1	8.86	8.08	9.2	8.42	8.08	4.1
95KZS4	36.2	8.89	8.33	6.5	8.89	8.13	8.9	8.35	8.12	2.8
94KZC4a	38.1	8.81	8.49	3.7	8.81	8.10	8.4	8.48	8.10	4.6
94KZC1	39.4	9.17	8.30	10.0	9.17	8.00	13.6	8.29	8.00	3.6
94KZC8	41.2	9.27	8.20	12.2	9.27	8.02	14.5	8.20	8.02	2.2
94KZSM1	48.1	8.80	8.48	3.7	8.80	8.09	8.4	8.49	8.09	4.8
ORKZC3	53.7	8.77	8.53	2.8	8.77	8.06	8.4	8.50	8.06	5.3
94KZS1	55.7	8.70	8.42	3.3	8.70	8.18	6.2	8.43	8.18	3.0
ORKZS6a	59.6	8.67	8.43	2.8	8.54	8.20	4.1	8.43	8.20	2.8
94KZSM6	63.4	8.57	8.46	1.3	8.57	8.27	3.6	8.44	8.27	2.0
ORKZC6	66.9	8.69	8.45	2.8	8.70	8.16	6.4	8.49	8.16	4.0
94KZSM3	68.1	8.73	8.50	2.7	8.73	8.10	7.5	8.52	8.10	5.1
94KZSM5	68.7	8.69	8.56	1.5	8.69	8.07	7.4	8.58	8.07	6.1
94KZSM7	69.4	8.68	8.52	1.9	8.68	7.96	8.7	8.53	7.96	6.9
Average	51.6	8.81	8.43	4.5	8.81	8.10	8.3	8.43	8.10	4.0

high temperatures and deformation associated with Neogene magmatic underplating and rifting. As mentioned earlier, strong reflections from the mafic lower crustal section of the region [*Giese*, 1995] also suggest the presence of horizontal fabrics in the vicinity of the Mohorovicic discontinuity. For this model, upper mantle olivine *a* axes are horizontal and strike N-S to NW-SE parallel to fast *Pn* velocities in the region (Figure 1).

The structure of the middle and lower lithosphere likely retains olivine orientation formed by Variscan convergence and imbrication. This major deformational event probably produced peridotite foliations with high angles of dip, similar to structures postulated to exist in many mantle regions which have undergone orogenic deformations associated with plate collisions [e.g., *Silver and Chan*, 1991]. The anisotropic signature of this convergence has remained fossilized in the mantle for the past 300 Myr and is recorded in the xenolith fabrics originating at depths below 45 km (Figures 6 and 8), as well as shear wave splitting observations (Figure 1).

As we noted, a comparison of regional shear wave splitting measurements with *Pn* anisotropy indicates that orientation of mineral fabrics in the middle to lower lithosphere differ from those in the upper lithosphere. To the south and north of the Ohře rift, vibration directions of the fast shear waves are approximately E-W and time differences between the shear wave arrivals range from 0.7 to 1.4s.

In Table 4 we summarize calculated shear wave properties for three possible fabric orientations of the Kozákov xenoliths. Listed for each sample, assuming vertical wave propagation, are the two shear wave velocities, shear anisotropy (ΔV_s, defined as the velocity difference in the two shear waves expressed as a percent of the mean velocity), and the thickness of an upper mantle slab necessary to produce a time difference in the arrivals of split shear waves. For peridotite xenoliths from depths below 45 km, the orientation models with horizontal foliation and vertical foliation (olivine *a* maxima vertical) have average ΔV_s of 2.0(±0.5)% and 2.4(±1.0)%, respectively, and assuming shear wave splitting to originate within the lithosphere, would require unreasonably high slab thicknesses of 263 and 243 km to produce a 1s difference in split shear wave arrival times. A significant increase in anisotropy in lower lithospheric regions, in which there is no xenolith control, would, however, lower estimated slab thicknesses. Our preferred model, in which foliation is vertical and olivine *c* maxima are vertical, has an average ΔV_s of 4.7(±0.8)% which requires a slab thickness of 109 km to produce 1s of shear wave splitting. For this model, olivine *a* axes in the middle and lower lithosphere are horizontal and strike approximately E-W, parallel to observed fast shear wave vibration directions in the region

9. Summary and Conclusions

An integrated study of xenolith mineral chemistry, geothermobarometry, petrofabric analysis, and geothermal modeling provides a detailed picture of the depth variations of upper mantle composition and anisotropy in central Europe (Figures 8 and 9). Temperatures obtained for 21 spinel lherzolite xenoliths from the Pliocene Kozákov volcano range from ~650 to ~1100°C. Although no viable geobarometer for spinel lherzolite presently exists, correlation of temperature estimates with a model geotherm at 5 Ma, the time of

Table 4. Shear Wave Velocity (V_s) Anisotropies for Vertical Shear Wave Propagation as a Function of Foliation Orientation

Sample	Depth, km	Horizontal Foliation (Olivine *b* Maxima Vertical)				Vertical Foliation (Olivine *c* Maxima Vertical)				Vertical Foliation (Olivine *a* Maxima Vertical)			
		V_s Fast km s^{-1}	V_s Slow km s^{-1}	ΔV_s %	1 s Slab km	V_s Fast km s^{-1}	V_s Slow km s^{-1}	ΔV_s %	1 s Slab km	V_s Fast km s^{-1}	V_s Slow km s^{-1}	ΔV_s %	1 s Slab km
94KZC13	32.5	4.92	4.74	3.7	130	4.93	4.74	3.9	123	4.93	4.92	0.2	2426
94KZS4	33.4	4.86	4.76	2.1	231	5.01	4.77	4.9	100	5.01	4.86	3.0	162
95KZS4	36.2	4.91	4.71	4.2	116	4.97	4.73	4.9	98	4.98	4.89	1.8	271
94KZC4a	38.1	4.85	4.75	2.1	230	4.98	4.76	4.5	108	4.98	4.85	2.6	186
94KZC1	39.4	4.95	4.64	6.5	74	4.97	4.63	7.1	68	5.01	4.92	1.8	274
94KZC8	41.2	4.94	4.59	7.3	65	5.00	4.61	8.1	59	5.00	4.94	1.2	412
94KZSM1	48.1	4.84	4.73	2.3	208	4.99	4.75	4.9	99	4.99	4.83	3.3	151
ORKZC3	53.7	4.84	4.77	1.5	330	5.02	4.76	5.3	92	5.02	4.84	3.7	135
94KZS1	55.7	4.86	4.77	1.9	258	5.02	4.78	4.9	100	5.02	4.86	3.2	152
ORKZS6a	59.6	4.90	4.80	2.1	235	4.94	4.79	3.1	158	4.94	4.87	1.4	344
94KZSM6	63.4	4.94	4.86	1.6	300	4.94	4.76	3.7	136	4.94	4.88	1.2	402
ORKZC6	66.9	4.89	4.79	2.1	234	4.98	4.79	3.9	126	4.99	4.89	2.0	244
94KZSM3	68.1	4.90	4.74	3.3	145	4.95	4.72	4.8	102	4.95	4.89	1.2	403
94KZSM5	68.7	4.83	4.76	1.5	328	5.04	4.76	5.7	86	5.04	4.83	4.3	116
94KZSM7	69.4	4.76	4.70	1.3	373	5.00	4.71	6.0	81	5.02	4.78	4.9	100
Average	51.6	4.88	4.74	2.9	217	4.98	4.74	5.0	113	4.99	4.87	2.4	385

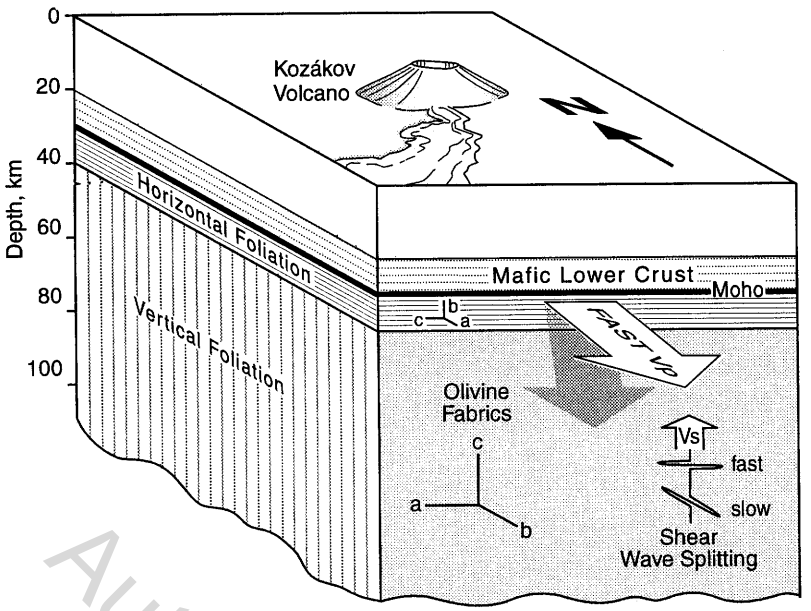

Figure 9. A structural model for upper mantle in the Lugian terrane of the Bohemian Massif, based on *Pn* anisotropy, *SKS* shear wave splitting observations, and xenolith fabrics and geothermobarometry.

extraction, suggests that the xenoliths originated from a continuous range of estimated depths between 32 and 70 km. The model estimated depths are thought to be a reasonable approximation to the actual depths of origin, because the model depths, which are derived from a plausible geological scenario, are compatible with phase petrology, constraints on maximum pressure from mineral compositions, and geothermal considerations. The Mg number of olivine and the Cr number of spinel decrease with increasing estimated depth, a feature that was most likely acquired by both equigranular and protogranular mantle prior to Variscan convergence and tectonic wedging.

The lithospheric mantle in this region has a layered structure (Figure 9). Olivine fabric data measured with the universal stage show orthorhombic symmetries and strong axes concentrations, giving rise to large seismic anisotropy for the uppermost lherzolites originating from 32 to 45 km depths. Below 45 km, olivine fabrics gradually change to axial, and seismic anisotropy decreases to a depth of 67 km. Below 67 km, anisotropy shows a slight increase with depth. This layered anisotropic structure correlates with lherzolite textures, which change from equigranular in the uppermost lithosphere (32-45 km) to protogranular (45-67 km) and back to equigranular (> 67 km).

Our integrated investigation reveals the complexity of the central European lithosphere. The uppermost mantle layer consists of lherzolite, whose fabric has been modified by Neogene rifting and heating related to magmatic underplating. A comparison of calculated *P* wave anisotropy for this uppermost layer with field-based *Pn* anisotropy observations indicates that foliation is horizontal, with olivine *a* axes horizontal and striking N-S to NW-SE, parallel to the fast *Pn* velocities in the region (Figure 9). For the middle and lower lithosphere, a comparison of shear wave splitting calculated for xenoliths and teleseismic observations indicate that foliation in lherzolite is vertical or steeply dipping, an orientation inherited from Variscan convergence, and olivine *a* axes are horizontal and strike approximately E-W, parallel to observed fast directions of shear wave splitting (Figure 9).

Acknowledgments. We thank Kim Schram, Bogie Soedjatmiko, and Chris Long for their contributions to the petrofabric analyses and Jon Zimmer for performing EMP analyses. Brian Hess provided high quality polished thin sections, and John Fournelle contributed invaluable advice and direction concerning analytical techniques. George Helffrich, Martha Savage, and David Mainprice contributed perceptive and constructive reviews that improved the paper. Financial support was provided by the National Science Foundation Continental Dynamics Program and a grant from the Ministry of Education, Czech Republic, J13/98:113100005.

References

Armstrong, J.T., Quantitative analysis of silicate and oxide materials: Comparison of Monte Carlo, ZAF, and φ(pz) procedures, *Microbeam Analysis, Proceedings of the 23rd Annual Conference* of the Microbeam Analysis Society, edited by D. E. Newbury, pp. 239-246, San Francisco Press, San Francisco, Calif., 1988.

Babuška, V., Elasticity and anisotropy of dunite and bronzitite, *J. Geophys. Res., 77*, 6955-6965, 1972.

Babuška, V., and J. Plomerová, The lithosphere in central Europe-Seismological and petrological aspects, *Tectonophysics, 207*, 141-163, 1992.

Babuška, V., J. Plomerová, and J. Šílený, Models of seismic anisotropy in the deep continental lithosphere, *Phys. Earth Planet. Inter., 78*, 167-191, 1993.

Baker, D.W., and N.L. Carter, Seismic velocity anisotropy calculated for ultramafic minerals and aggregates; in *Flow and Fracture of Rocks, Geophys. Monogr. Ser.*, vol. 16, edited by H. Heard et al., pp. 157-166, AGU, Washington, D. C., 1972.

Ballhaus, C., R.F. Berry, and D.H. Green, High pressure experimental calibration of the olivine-orthopyroxene-spinel oxygen geobarometer: Implications for the oxidation state of the upper mantle, *Contrib. Mineral. Petrol., 107*, 27-40, 1991.

Bamford, D., *Pn* velocity anisotropy in a continental upper mantle, *Geophys. J. R. Astron. Soc., 49*, 29-48, 1977.

Ben Ismail, W., and D. Mainprice, An olivine fabric database: An overview of upper mantle fabrics and seismic anisotropy, *Tectonophysics., 296*, 145-157, 1998.

Bertrand, P., and J.-C.C. Mercier, The mutual solubility of coexisting

ortho- and clinopyroxene: toward an absolute geothermometer for the natural system?, *Earth Planet. Sci. Lett., 76,* 109-122, 1985.

Bormann, P., G. Gruenthal, R. Kind, and H. Montag, Upper mantle anisotropy beneath central Europe from *SKS* wave splitting; effects of absolute plate motion and lithosphere-asthenosphere boundary topography? *J. Geodyn., 22,*11-32, 1996.

Brey, G.P., and T. Köhler, Geothermobarometery in four-phase lherzolites. II. New thermobarometers and practical assessment of existing thermobarometers, *J. Petrol., 31,* 1352-1378, 1990.

Carswell, D.A., Variscan high P-T metamorphism and uplift history in the Moldanubian Zone of the Bohemian Massif in lower Austria, *Eur. J. Mineral., 3,* 323-342, 1991.

Carter, N.L., and H.G. Ave'Lallemant, High temperature flow of dunite and peridotite, *Geol. Soc. Am. Bull., 81,* 2181-2202, 1970.

Čermák, V., Crustal heat production and mantle heat flow in central and eastern Europe, *Tectonophys., 159,* 195-215, 1989.

Čermák, V., M. Král, M. Krešl, J. Kubík, and J. Šafanda, Heat flow, regional geophysics, and lithosphere structure in Czechoslovakia and adjacent parts of central Europe, in *Terrestrial Heat Flow and Lithosphere Structure,* edited by V. Čermak, and L. Rybach, pp. 33-165, Springer-Verlag, New York, 1991.

Christensen, N.I., Elasticity of ultrabasic rocks, *J. Geophys. Res., 71,* 5921-5931, 1966.

Christensen, N.I., The magnitude, symmetry and origin of upper mantle anisotropy based on fabric analyses of ultramafic tectonites, *Geophys. J. R. Astron. Soc., 76,* 89-111, 1984.

Christensen, N.I., and R.S. Crosson, Seismic anisotropy in the upper mantle, *Tectonophysics, 6,* 93-107, 1968.

Christensen, N.I., and S.M. Lundquist, Pyroxene orientation within the upper mantle, *Geol. Soc. Am. Bull., 93,* 279-288, 1982.

Christensen, N.I., and R. Ramananantoandro, Elastic moduli and anisotropy of dunite to 10 kilobars, *J. Geophys. Res., 76,* 4003-4010, 1971.

Christensen, N.I., and M.H. Salisbury, Seismic anisotropy in the oceanic upper mantle: Evidence from the Bay of Islands Ophiolite complex, *J. Geophys. Res., 84,* 4601-4610, 1979.

Cloetingh, S., and E. Banda, Mechanical Structure, in *A Continent Revealed,* edited by D. Blundell, R. Freeman, and S. Mueller, pp. 80-91, Cambridge Univ. Press, New York, 1992.

Costa, S., and P. Rey, Lower crustal rejuvenation and growth during post-thickening collapse: Insights from a crustal cross section through a Variscan metamorphic core complex, *Geology, 23,* 905-908, 1995.

Crosson, R.S., and J.W. Lin, Voigt and Reuss prediction of anisotropic elasticity of dunite, *J. Geophys. Res., 76,* 570-578, 1971.

Cull, J.P., S.Y. O'Reilly, and W.L. Griffin, Xenolith geotherms and crustal models in eastern Australia, *Tectonophysics, 192,* 359-366, 1991.

Echtler, H.P., E. Lueschen, and G. Mayer, Lower crustal thinning in the Rhinegraben: implications for Recent rifting, *Tectonics, 13,* 342-353, 1994.

Emmons, R.C., The Universal Stage, *Mem. Geol. Soc. Am., 8,* 205 pp., 1943.

Evans, B., and D.L. Kohlstedt, Rheology of rocks, in Rock Physics and Phase Relations, *AGU Ref. Shelf,* vol. 3, edited by T.J. Ahrens, pp. 148-165, AGU, Washington, D. C., 1995.

Farsky, F., Mineralogische Notizen, 1, Mineralien aus den Kosakover Basltkugeln, *Verh. Geol.* Bundesanst., 205-208, 1876.

Fediuk, F., Ultramafity Krkonošsko-Jizerské oblasti, *Acta Univ. Carol. Geol., 4,* 310-343, 1971.

Fediuk, F., Deep-origin xenoliths in volcanics of Czechoslovakia, in *Crustal Structure of the Bohemian Massif and the West Carpathians,* edited by V. Bucha and M. Blížkovský, pp. 277-281, Springer-Verlag, New York, 1994.

Franke, W., R.D. Dallmeyer, and K. Weber, Geodynamic evolution, in *Pre-Permian Geology of Central and Eastern Europe,* edited by R.D. Dallmeyer, W. Franke, and K. Weber, pp. 579-593, Springer-Verlag, New York, 1995.

Frey, F.A., and M. Prinz, Ultramafic inclusions from San Carlos, Arizona, petrologic and geochemical data bearing on their petrogenesis, *Earth Planet. Sci. Lett., 38,* 129-176, 1978.

Giese, P., Main features of geophysical structures in central Europe, in *Pre-Permian Geology of Central and Eastern Europe,* edited by R.D. Dallmeyer, W. Franke, and K. Weber, pp. 7-25, Springer-Verlag, New York, 1995.

Griffin, W.L., A. Zhang, S.Y. O'Reilly, and C.G. Ryan, Phanerozoic evolution of the lithosphere beneath the Sino-Korean Craton, in *Mantle Dynamics and Plate Interactions in East Asia, Geodyn. Ser.,* vol. 27, edited by M.F.J. Flower et al., pp. 107-126, AGUnion, Washington, D. C., 1998

Jakeš, P., and E. Jelínek, Granulites of the Bohemian Massif: A bag with two stories, *J. Czech Geol. Soc., 42,* 58, 1997.

Ji, S., X. Zhao, and D. Francis, Calibration of shear-wave splitting in the subcontinental upper mantle beneath active orogenic belts using ultramafic xenoliths from the Canadian Cordillera and Alaska, *Tectonophysics, 239,* 1-27, 1994.

Kasinski, J.R., Tertiary lignite-bearing lacustrine facies of the Zittau Basin: Ohře rift system (Poland, Germany and Czechoslovakia), *Spec. Publ. Int. As. Sedimentol., 13,* 93-107, 1991.

Kern, H., L. Burlini, and I.V. Ashchepkov, Fabric-related seismic anisotropy in upper-mantle xenoliths: Evidence from measurements and calculations, *Phys. Earth Planet. Inter., 95,* 195-209, 1996.

Klíma, K., and V. Babuška, A comparison of measured and calculated elastic anisotropies of mantle, *Stud. Geophys. Geod., 12,* 377-384, 1968.

Köhler, T.P., and G.P. Brey, Calcium exchange between olivine and clinopyroxene calibrated as a geothermobarometer for natural peridotites from 2 to 60 kb with applications, *Geochim. Cosmochim. Acta, 54,* 2375-2388, 1990.

Kopecký, L., Geological development and block structure of the Cenozoic Ohře Rift (Czechoslovakia), in *Proceedings of the 6th International Conference on Basement Tectonics,* edited by M.J. Aldrich, Jr. And A.W. Laughlin, pp. 114-124, 1986.

Kumazawa, M., The elastic constants of rock in terms of elastic constants of constituent mineral grains, petrofabric and interface structures, *J. Earth Sci., 72,* 147-176, 1964.

Kumazawa, M., The elastic constants of single-crystal orthopyroxene, *J. Geophys. Res., 74,* 5973-5980, 1969.

Kumazawa, M., and O.L. Anderson, Elastic moduli, pressure derivatives, and temperature derivatives of single-crystal olivine and single-crystal forsterite, *J. Geophys. Res., 74,* 5961-5972, 1969.

Levin, V., W. Menke, and J. Park, Shear wave splitting in the Appalachians and the Urals: A case for multilayered anisotropy, *J. Geophys. Res., 104,* 17975-17993, 1999.

Lorenz, V., and I.A. Nicholls, The Permocarboniferous basin and range province of Europe: An application of plate tectonics, in *The Continental Permian in Central, West, and south Europe, NATO ASI Series C,* vol. 22, edited by H. Falke, pp. 313-342, D. Reidel, Norwell, Mass., 1976.

Mainprice, D., and P.G. Silver, Interpretation of *SKS*-waves using samples from the sub continental lithosphere, *Phys. Earth Planet. Inter., 78,* 257-280, 1993.

Makeyeva, L.I., L.P. Vinnik, and S.W. Roecker, Shear-wave splitting and small-scale convection in the continental upper mantle, *Nature, 358,* 144-147, 1992.

Malkovský, M., The Mesozoic and Tertiary basins of the Bohemian Massif and their evolution, *Tectonophysics, 137,* 31-42, 1987.

Medaris, L.G., Jr., H.F. Wang, Z. Mísař and E. Jelínek, Thermobarometry, diffusion modelling and cooling rates of crustal garnet peridotites: two examples from the Moldanubian zone of the Bohemian Massif, *Lithos, 25,* 189-202, 1990.

Medaris, L.G. Jr., J.H. Fournelle, H.F. Wang, and E. Jelínek, Thermobarometry and reconstructed chemical compositions of spinel-pyroxene symplectites: Evidence for pre-existing garnet in lherzolite xenoliths from Czech Neogene lavas, *Russ. Geol. Geophys., 38,* 277-286, 1997.

Medaris, L.G., Jr., H.F. Wang, J.H. Fournelle, J.H. Zimmer, and E. Jelínek, A cautionary tale of spinel peridotite thermobarometry: An example from xenoliths of Kozákov volcano, Czech Republic, *Geolines, 9,* 92-96, 1999.

Mercier, J-C.C., and A. Nicolas, Textures and fabrics of upper-mantle peridotites as illustrated by xenoliths from basalts, *J. Petrol., 16,* 454-487, 1975.

Musgrave, M.J.P., *Crystal Acoustics,* Holden-Day, Merrifield, Va., 1970.

Nicolas, A., and N.I. Christensen, Formation of anisotropy in upper mantle peridotites; a review, in *Composition, Structure and Dynamics of the Lithosphere-Asthenosphere System, Geodyn. Ser.,* vol. 16, edited by K. Fuchs, and C. Froidevaux, pp. 111-123, AGU, Washington, D. C., 1987.

Nicolas, A., F. Boudier, and A.M. Boullier, Mechanisms of flow in naturally and experimentally deformed peridotites, *Am. J. Sci., 273*, 853-876, 1973.

O'Neill, H.St.C., The transition between spinel lherzolite and garnet lherzolite, and its use as a geobarometer, *Contrib. Mineral. Petrol., 77*, 185-194, 1981.

O'Reilly, S.Y., D. Chen, W.L. Griffin, and C.G. Ryan, Minor elements in olivine from spinel lherzolite xenoliths: Implications for thermobarometry, *Mineral. Mag., 61*, 257-269, 1996.

Ozalaybey, S., and M.K. Savage, Double-layer anisotropy resolved from *S* phases, *Geophys. J. Int., 117*, 653-664, 1994.

Panza, G.F., Lateral variations in the lithosphere in correspondence of the southern segment of EGT, in *Second EGT Workshop: The Southern Segment*, pp. 47-51, Eur. Sci. Found., Strasbourg, France, 1985.

Peselnick, L., J.P. Lockwood, and R. Stewart, Anisotropic elastic velocities of some upper mantle xenoliths underlying the Sierra Nevada batholith, *J. Geophys. Res., 82*, 2005-2010, 1977.

Plomerová, J., V. Babuška, and J. Horálek, Seismic anisotropy and velocity variation in the mantle beneath the Saxothuringicum-Moldanubicum contact in central Europe, *Pure Appl. Geophys., 151*, 365-394, 1998.

Ranalli, G., *Rheology of the Earth*, 2nd ed., 413 pp., Chapman and Hall, New York, 1995.

Rey, P., Seismic and tectonometamorphic characters of the lower continental crust in Phanerozoic areas: A consequence of post-thickening extension, *Tectonics, 12*, 580-590, 1993.

Sandvol, E., J. Ni, S. Ozalaybey, and J. Schlue, Shear-wave splitting in the Rio Grande Rift, *Geophys. Res. Lett., 19*, 2337-2340, 1992.

Savage, M.K., Seismic anisotropy and mantle deformation: What have we learned from shear wave splitting?, *Rev. Geophys., 37*, 65-106, 1999.

Savage, M.K., and P.G. Silver, Mantle deformation and tectonics: constrains from seismic anisotropy in the western United States, *Phys. Earth Planet. Inter., 78*, 207-227, 1993.

Šibrava, V., and P. Havlíček, Radiometric age of Plio-Pleistocene volcanic rocks of the Bohemian Massif, *Věst. Ústr. Úst. Geol., 55*, 129-139, 1980.

Silver, P.G., Seismic anisotropy beneath the continents; probing the depths of geology, *Annu. Rev. Earth Planet. Sci., 24*, 385-432, 1996.

Silver, P.G., and W.W. Chan, Implications for continental structure and evolution from seismic anisotropy, *Nature, 335*, 34-39, 1988.

Silver, P.G., and W.W. Chan, Shear wave splitting and subcontinental mantle deformation, *J. Geophys. Res., 96*, 16,429-16,454, 1991.

Smith, G.P., and G. Ekstrom, A global study of *Pn* anisotropy beneath continents, *J. Geophys. Res., 104*, 963-980, 1999.

Suzuki, I., and O.L. Anderson, Elasticity and thermal expansion of a natural garnet up to 1000K, *J. Phys. Earth, 31*, 125-138, 1983.

Ulrych, J., E. Pivec, M. Lang, K. Balogh, and V. Kropáček, Cenozoic intraplate volcanic rock series of the Bohemian Massif: A review, *Geolines, 9*, 123-129, 1999.

Verma, R.K., Elasticity of some high-density crystals, *J. Geophys. Res., 65*, 757-766, 1960.

Vinnik, L.P., L.I. Makeyeva, A. Milev, and A. Yu Usenko, Global patterns of azimuthal anisotropy and deformations in the continental mantle, *Geophys. J. Int., 111*, 433-447, 1992.

Vinnik, L.P, V.G. Krishna, R. Kind, P. Bormann, and K. Stammler, Shear wave splitting in the records of the German Regional Seismic Network, *Geophys. Res. Lett., 21*, 457-460, 1994.

Vokurka, K., and P. Povondra, Geothermometry and geobarometry of lherzolite nodules from Kozákov, NE Bohemia, Czechoslovakia, *Acta Univ. Carol. Geol., 4*, 261-272, 1983.

Witt-Eickschen, G., and H.A. Seck, Solubility of Ca and Al in orthopyroxene from spinel peridotite: An improved version of an empirical geothermometer, *Contrib. Mineral. Petrol.*, 106, 431-439, 1991.

Zhang, S., S. Karato, J.F. Gerald, V.H. Faul, and Y. Zhou, Simple shear deformation of olivine aggregates, *Tectonophysics, 316*, 133-152, 2000.

Ziegler, P.A., European Cenozoic rift system, *Tectonophysics, 208*, 91-111, 1992.

N.I. Christensen, L.G. Medaris Jr., and H. F. Wang, Department of Geology and Geophysics, University of Wisconsin-Madison, 156 Weeks Hall, 1215 West Dayton St., Madison, WI 53706. (chris@geology.wisc.edu)

E. Jelínek, Institute of Geochemistry, Mineralogy and Mineral Resources, Charles University, Albertov 6, 12843 Prague 2, Czech Republic.

(Received January 24, 2000; revised July 28, 2000; accepted September 6, 2000.)